CHAPTER X

STEREO CHEMISTRY AND ELECTRONIC STRUCTURE XAFS SPECTROSCOPY: DATA-ANALYSIS AND APPLICATIONS

D.C. KONINGSBERGER[1]

X. Introduction

The structural and electronic characterization of a material provides a basic understanding of its properties. Traditionally, diffraction techniques (XRD, neutron diffraction, LEED) are being used for most of the structural investigations and reliable structures can be determined for materials that exhibit a long-range structural order (like single crystals or polycrystalline material). X-ray Absorption Fine Structure (XAFS) spectroscopy is a powerful technique to characterize all forms of matter irrespective of their degree of crystallinity. EXAFS (Extended X-ray Absorption Fine Structure spectroscopy probes the local structure of a material. The local structure of highly disordered solids, amorphous materials and liquids can be unraveled with EXAFS. In addition, the chemical state and the electronic properties can be determined from the X-ray Absorption Near Edge Structure (XANES) which extends within 40 eV of the X-ray absorption edge. One of the major advantages of XAFS is its atomic selectivity which enables the investigation of the local structure of each different constituent of a sample. As shown by Fontaine (1993), the recent availability of high-brightness synchrotron radiation sources has resulted in a prosperous development XAFS spectroscopy.

Fontaine has extensively discussed in chapter XV of volume I of this edition the underlying physical principles of XAFS. Here the basic concepts of the analysis of XAFS data will be given. These concepts are very general and therefore important for the application of EXAFS in the fields of coordination chemistry, catalysis, bio-inorganic chemistry, biology, surface physics and chemistry. EXAFS have been widely used to determine the stereo chemistry of inorganic compounds. To illustrate the importance of XAFS spectroscopy applications in the field of inorganic chemistry are extremely useful. Inorganic materials are the building stones of an important class of compounds called catalysts. Most industrial catalysts consist of metal, metal-oxides or metal-sulfides particles dispersed on high-area supports exposing most of the particle surface to reactants. Highly dispersed supported metal catalysts are used for chemical processes like hydrogenation, hydrotreating, hydrocracking and catalytic reforming. The particles are stabilized by metal-support interactions that hinder particle migration, coalescence, and loss of catalytic activity by loss of metal surface area. Metal-support interactions also affect the activities of catalysts, and extensive research has been done to elucidate the effects. However, only little is understood about the nature of the metal-support interface or the role of the support in influencing the reactivity of supported metal particles. Metal-oxides are mostly

---

1 The unpublished results in this chapter are taken from M. Vaarkamp, thesis 1993 and F.W.H. Kampers, thesis 1988, Eindhoven University of Technology, The Netherlands.

used for oxidation reactions, while metal-sulfides are detrimental for the removal of sulfur from oil feedstocks. Metal-oxides and sulfides can be dispersed as monolayers onto the support. The understanding of particle size and support effects are limited by the lack of precise methods for structural characterization of supported catalytic particles and the particle-support interface, combined with the nonuniformity of the available samples. Extremely high dispersed material consisting of particles built up by only a small number of atoms can not be studied by techniques like X-ray diffraction or Transmission Electron Microscopy. EXAFS can be tuned to study the different constituents of a catalytic system. It can be used to study in detail the particle-support interface. It is possible with *in-situ* techniques to follow the change in electronic properties and the structure due to the absorption of reactants on the surface. The X-ray absorption edge can give additional information about local chemistry and electronic structure (XANES, see also Fontaine chapter XV volume 1 of this edition).

This chapter will show how important XAFS spectroscopy is for the study of catalytic materials mostly consisting of inorganic compounds. The very important property of XAFS spectroscopy which is that experiments can be performed *in-situ* will be demonstrated. In section X.2 important aspects of the analysis of EXAFS data will be discussed. An important example of the determination with the EXAFS technique of the stereo chemistry in catalytic materials will be discussed in section X.3. EXAFS has been used to determine the structure of the metal-support interface of extremely small iridium clusters supported on MgO. This information is very important for a fundamental understanding of catalytic properties. Section X.4 deals with the determination of the electronic structure of small platinum metal particles. The electronic properties of small metal particles are of interest from fundamental standpoint of view. More information is needed to interprete and understand XPS data published in the literature. Moreover, the determination of the electronic structure is important for an understanding of the properties of catalytic materials. It will be shown that the white-line intensity of the L_{II} and L_{III} absorption edges can be used to measure the local d-band density of states of transition metal atoms.

X.2. EXAFS Data-Analysis

X.2.1. EXAFS Equation

An accurate theoretical description of EXAFS spectra includes curved wave effects and an energy dependent self-energy (McKale et al., 1988; Vaarkamp (1) et al., 1993). The curved wave EXAFS formula (Ashley et al., 1975; Lee et al., 1975, Stern et al., 1975) can be reduced to the plane-wave EXAFS formula (eq. X.1 and X.2) without loss of accuracy, if the model function used in the data-analysis procedure is based upon the use of a reference absorber-backscatterer coordination (obtained experimentally or theoretically) having approximately the same distance as the coordination in the unknown material

$$\chi(k) = \sum_{j=1}^{Shells} A_j(k) \sin\left[2kR_j + \varphi_j(k)\right]. \qquad \text{(X.1)}$$

with R_j being the coordination distance and $\varphi_j(k)$ being the phase function determined by both the absorber and backscatterer. The amplitude $A_j(k)$ can be expressed as:

$$A_j(k) = \frac{S_0^2 e^{-2R_j/\lambda}}{kR_j^2} \bullet N_j F_j(k) \bullet e^{-2\sigma_j^2 k^2} . \qquad \text{(X.2)}$$

damping scattering disorder
power

The first group of terms describes the damping of the electron wave: the exponential term $e^{-2R_j/\lambda}$ accounts for the finite lifetime of the excited state and $S_0^2(k)$ is an amplitude reduction factor which accounts for the photo-electron energy loss due to many body effects and shake-up/shake-off processes in the absorber atom (not all the energy of the impinging photon is transferred to the photo-electron). The second group of terms is characteristic for the scattering power experienced by the reflected electron wave: $F_j(k)$ is the back-scattering amplitude of the neighbouring atoms and N_j is the average coordination number in the jth shell. The third term contains the Debye-Waller factor σ_j which represents the root mean square fluctuation in R_j caused by thermal motion of the atoms and the structural disorder present in the material.

Equations X.1 and X.2 are being used to analyze EXAFS data. The final goal is to determine from the experimental data the coordination distance R_j, the coordination number N_j and the Debye-Waller factor σ_j for each individual coordination shell. EXAFS can distinguish between different types of neighbouring atoms. As an example the phase shift of the Pt-Pt and Pt-O absorber-backscatterer pair and the backscattering amplitude of O and Pt are plotted in Fig. X.1a and X.1b, respectively. It can be seen that both the Pt-Pt and the Pt-O phases are a non-linear function of k. The backscattering amplitude of oxygen (typical low Z scatterer) is decaying rapidly with increasing values of k, whereas the amplitude of platinum (typical high Z scatterer) is still significant at high values of k.

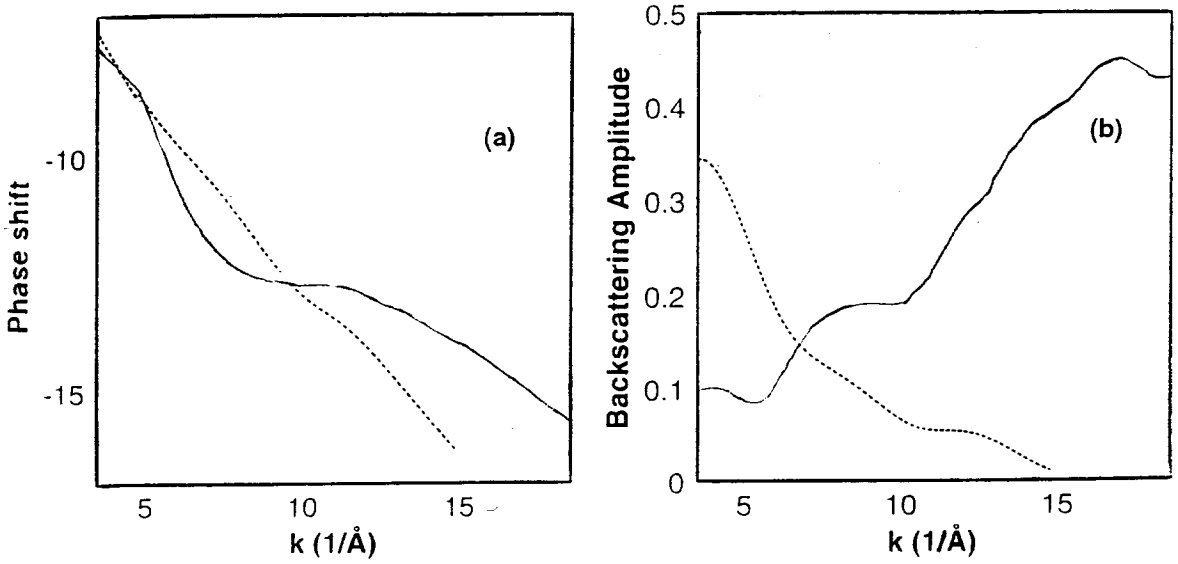

Figure X.1. — a) Phase shift $(\varphi(k))$ and b) Backscattering amplitude $(F(k))$ of Pt-Pt (solid line) and Pt-O (dotted line). Data were obtained from first shell EXAFS data of Pt foil and $Na_2Pt(OH)_6$.

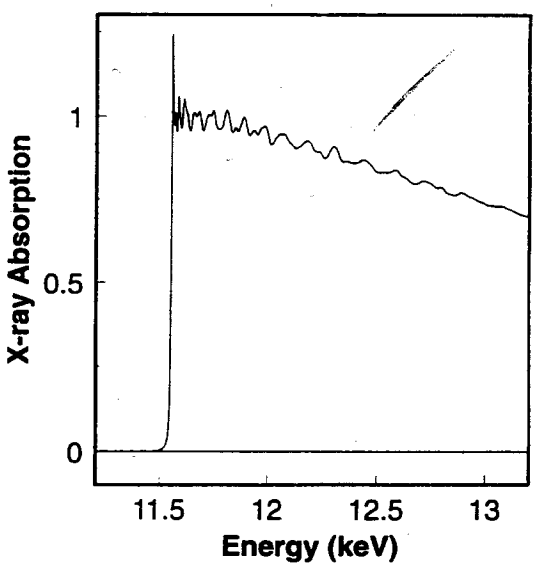

Figure X.2. — Isolated X-ray absorption spectrum of a 4 μ Pt-foil measured at 77K on beamline 9.2 SRS Daresbury.

X.2.2. Extraction of the EXAFS Function

The first step in the analysis of an XAFS spectrum is to separate the XAFS oscillations from the experimentally measured X-ray absorption coefficient. The necessary steps for the extraction of the EXAFS function are: (i) pre-edge subtraction, (ii) determination of inner potential value, (iii) post-edge background subtraction, (iv) normalisation (Sayers et al., 1988). A standard procedure to remove the pre-edge absorption involves fitting the spectrum in the energy range sufficiently below the absorption edge (typically - 200 to - 40 eV) with a polynomial. The fitted polynomial is extrapolated past the edge and subtracted from the entire spectrum. This step removes the absorption due to all other electrons and isolates the contribution of a particular absorption edge from the total absorption. Figure X.2 gives the isolated X-ray absorption of a 4μ thick platinum foil measured at liquid nitrogen temperature at the EXAFS station 9.2 of the SRS, Daresbury, UK.

The next step consist of removing the smoothly varying post-edge background μ_0 by fitting the post-edge region (typically starting at 20 eV above the edge) with a spline function and subtracting it from the data (Cook et al., 1981). The EXAFS function is then normalized on a per atom basis by dividing the data through the edge jump μ_0 at the absorption edge (Sayers et al, 1988). The normalized EXAFS function is converted to k-space by using:

$$k = \left[\left(\frac{8\pi^2 m}{h^2}\right)(h\nu - E_0)\right]^{1/2}. \qquad \text{(X.3)}$$

In the initial stage of analysis, the value of E_0 is chosen at the maximum derivative point on the edge. At later stages, E_0 is varied and adjusted to its proper value. The normalized EXAFS spectrum of the platinum foil is shown in Fig. X.3a.

X.2.3. Fourier Filtering: Separation of Coordination Shells

As discussed above the EXAFS function shown in Fig. X.3a is a superposition of a number of damped sinusoidal functions, each corresponding to a particular

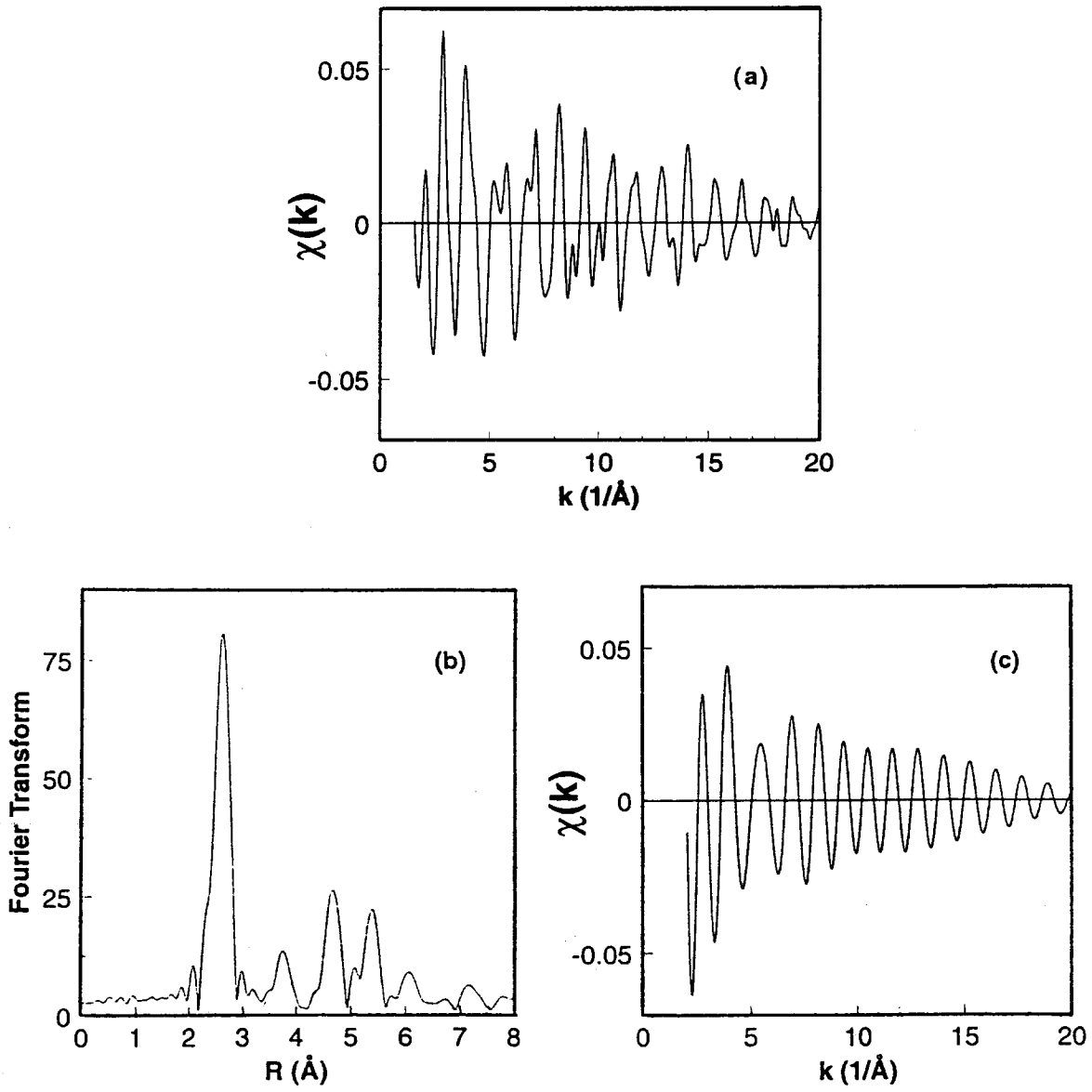

Figure X.3. — a) EXAFS spectrum of Pt foil obtained after background subtraction and normalisation. b) Fourier transform; k^3, Δk: 2.2 - 20.3 $Å^{-1}$. c) Isolated first shell EXAFS; ΔR: 1.1 - 3.1 Å.

coordination shell. Fourier transformation of $\chi(k)$ yields peaks in r-space corresponding to individual coordination shells around the absorbing atom (Sayers et al., 1988):

$$FT(r) = \frac{1}{\sqrt{2\pi}} \int_{k_{min}}^{k_{max}} k^n \chi(k) e^{-2ikr} dk. \qquad \text{(X.4)}$$

The peaks are shifted to lower r-values from the real interatomic distances due to the influence of the phase shift function. The weight factor k^n can be used to compensate for the decay in amplitude of the spectrum with increasing values of k or to emphasize a particular part of the EXAFS spectrum. The Fourier transform of the platinum foil EXAFS spectrum is shown in Fig. X.3b.

The EXAFS function of a particular coordination shell can now be isolated by applying a window in r-space and performing an inverse Fourier transform to k-space (Sayers et al., 1988):

$$k^n\chi_j(k) = \frac{1}{\sqrt{2\pi}}\int_{R_{min}}^{R_{max}} FT(r)\, e^{-2ikr}\, dr. \qquad \text{(X.5)}$$

This step produces a modulated sinusoidal function with amplitude $A_j(k)$ and argument $\Phi_j(k) = 2kR_j + \varphi_j(k)$, as given in Eq. X.1. The isolated EXAFS function for the first shell of platinum foil is shown in Fig. X.3c. $A(k)$ and $\Phi(k)$ for a particular coordination shell can now be obtained in tabular form from an EXAFS experiment.

X.2.4. Non-linear Least Square Multiple Shell Fitting

To extract the coordination parameters R, N and σ from the EXAFS data the quantities $\varphi(k)$, S_0^2, $e^{(-2R/\lambda)}$ and $F(k)$ have to be known. It is now generally accepted that the phase shift $\varphi(k)$ and $F(k)$ are transferable from the reference compound to the compound with unknown structure. The argument $\Phi_r(k)$ and amplitude $A_r(k)$ of an absorber-backscatterer pair can be extracted by Fourier filtering of an EXAFS spectrum (as shown in section X.2.3) from a reference compound (with a well defined known structure) in which the contributions are well separated. The phase shift can be obtained by $\varphi(k) = \varphi_r(k) = \Phi_r(k) - 2kR_r$. To determine $F(k)$ one still has to know input values for S_0^2 and $e^{(-2R/\lambda)}$. To circumvent this requirement we assume that not only $\varphi(k)$ and $F(k)$ but also S_0^2 and $e^{(-2R/\lambda)}$ are transferable from one compound to another. The validity of this assumption has been shown for compounds with the same absorber-backscatterer pair (Citrin et al., 1976; Bunker et al., 1983) but even for absorbers or backscatterers which are neighbours in the periodic table (Teo et al., 1997; Lengeler, 1986). This leads to the definition of a modified backscattering amplitude $F'(k)$ (Vaarkamp (2), 1993):

$$F'(k) = S_0^2 e^{(-2R/\lambda)} e^{-2k^2\sigma^2} F(k). \qquad \text{(X.6)}$$

This modified backscattering amplitude contains the Debye-Waller factor of the reference compound. Hence, the Debye-Waller factor ($\Delta\sigma^2$) obtained from the data-analysis is relative to the Debye-Waller factor of the reference compound. This modified backscattering amplitude $F'(k)$ can now be derived from the measured amplitude $A_r(k)$ of the Fourier filtered EXAFS of the reference compound by:

$$F'(k) = F'_r(k) = \frac{kR_r^2}{N_r} \bullet A_r(k). \qquad \text{(X.7)}$$

The function to be minimized with a non-linear least square refinement becomes (Vaarkamp (2), 1993):

$$\chi_{exp}(k) - \sum_{j=1}^{Shells} \frac{N_j}{k'_j R_j^2} e^{-2k'^2_j \Delta\sigma_j^2} F'_j(k'_j) sin\left[2k'_j R_j + \varphi_j(k'_j)\right]. \qquad (X.8)$$

Here k' is the photo electron wave vector corrected for the difference in inner potential (ΔE_0) between the sample and the reference compound:

$$k' = \sqrt{k^2 + \frac{4\pi m}{h} \Delta E_0}. \qquad (X.9)$$

Generally, $F'(k')$ and $\varphi(k')$ are not known at the values of k' where $\chi_{exp}(k)$ has been measured due to different experimental setup or a shift in k' value due to a change in ΔE_0. As ΔE_0 is a fitting parameter, the values of k', and consequently $F'(k')$ and $\varphi(k')$ are subject to change during a refinement.

Overlapping coordination shells have to be isolated by inverse Fourier transformation and a multiple shell non-linear least square fitting routine has to be applied. The structural parameters N, R and $\Delta\sigma^2$ have to be refined for every contribution (shell). In deriving eq. X.1 one assumes the presence of a Gaussian pair-distribution function and small disorder. If the pair-distribution function is not Gaussian and if the system is highly disordered, the standard data analysis procedure described here is not valid (Crozier et al., 1988).

X.2.5. The Use of Phase Shifts and Backscattering Amplitudes Obtained from Theory

As shown in the previous section, the phase shift $\varphi(k)$ and the backscattering amplitude $F(k)$ can be extracted by Fourier filtering from the EXAFS spectrum of a compound with known structure. They can also be calculated from first principles. Both methods can introduce (systematic) errors in the analysis of unknown compounds. Extraction of backscattering amplitudes and phase shifts from reference compounds suffers from Fourier filtering truncation errors. The accuracy of calculated backscattering amplitudes and phase shifts is hampered by the approximations necessary to make calculations possible. A number of first principle methods to calculate backscattering amplitudes and phase shifts have been developed (Pendry et al., 1974; Teo et al., 1979; McKale et al., 1986; Binsted et al., 1987; Mustre de Leon et al., 1991). Computer programs as EXCURV and FEFF are being widely used, while the tables of phase shifts and backscattering amplitudes as compiled by Teo and Lee, and McKale are applied as well.

One of the goals of the International Committee on Standards and Criteria in X-ray Absorption Spectroscopy (Lytle et al., 1988) is to assess quantitatively the applicability of current theoretical models in XAFS analysis. Vaarkamp (1) et al., 1993 has carried out a systematic investigation to compare the phase shifts and backscattering amplitudes obtained from high quality EXAFS data of reference compounds with those calculated from first principles. The theoretical standards were based on different prescriptions for scattering potentials and self-energies or exchange potentials. The most straightforward way of comparing calculated and experimental XAFS is by looking at a single absorber-backscatterer pair in a single scattering process. Only mono-atomic metals were used to avoid the difficulties of charged atoms in calculations. From each of the first three rows of the transition metals a readily available compound was selected (Cu, Rh, and Pt foil respectively).

The separation of the single scattering first shell contribution from the complete EXAFS spectrum was carried out by Fourier filtering. The Fourier filtering suffers from truncation errors due to the limited data range used in both the forward and the inverse Fourier transform. To verify that Fourier filtering introduces errors which are negligible compared to the differences in the theoretical standards Vaarkamp (1) et al., 1993 carried out a model study to quantify the Fourier filtering errors, which is summarized in section X.2.5.1. From the statistical errors in the data and the differences between experimental data and fit (based on theoretically obtained phase shifts and backscattering amplitudes), goodness of fit values and errors in the determined parameters are calculated. The goodness of fit values and the number of free parameters are used to test whether the differences in fit quality between the different theoretical references are statistically significant.

X.2.5.1. Fourier Filtering Truncation Errors

To quantify the errors made by Fourier filtering a test single (first) shell copper foil EXAFS spectrum was calculated with the phase shift and backscattering

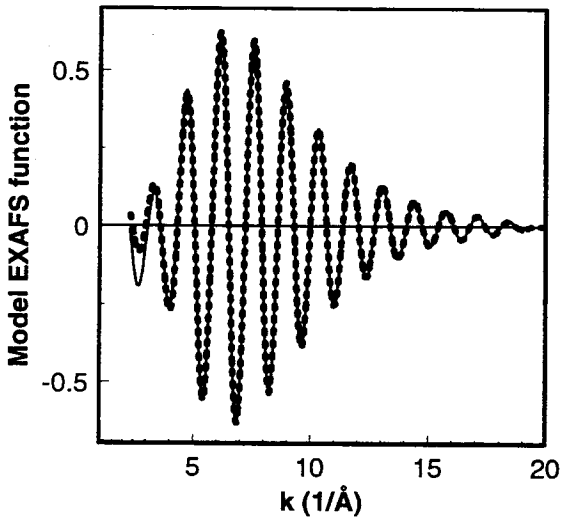

Figure X.4. — Model EXAFS function (solid line) calculated from theory (FEFF) with N=12, R=2.56 Å., σ^2= 0.0033. Dotted line is obtained by Fourier filtering of model EXAFS function; k^3, Δk: 2.3 - 19.4 $Å^{-1}$, ΔR: 1.3 - 3.1 Å.

amplitude obtained with FEFF. This test single shell EXAFS spectrum was Fourier filtered over a number of forward and inverse ranges. By analyzing the Fourier filtered EXAFS spectrum with the phase shift and backscattering amplitude used to calculate the original test first shell EXAFS spectrum, filtering errors were quantified. The agreement between the original test first shell EXAFS and the Fourier filtered spectrum is expressed as the k^n variance:

$$k^n \text{ variance} = 100 \frac{\int \left\{ k^n \left(\chi_{\text{model}}(k) - \chi_{\text{exp}}(k) \right) \right\}^2}{\int \left\{ k^n \chi_{\text{exp}}(k) \right\}^2} \qquad \text{(X.10)}$$

As Fourier truncation errors in the Fourier filtered EXAFS spectrum are largest at the start and end of the forward Fourier transform interval the range and weighing of analysis were varied. To see the effect of window functions, forward transforms ending and starting at nodes or maxima and minima were compared. Analysis of a Fourier filtered function obtained with a forward range of Δk: 2.3 - 19.4 $Å^{-1}$ and an inverse range of Δr: 0-8 Å resulted in a variance of zero, implying that in this case Fourier filtering errors do not occur. Analysis of a Fourier filtered EXAFS function obtained with a forward range of Δk: 2.3 - 19.4 $Å^{-1}$ and an inverse range of Δr: 1.3 - 3.1 Å resulted in a non-zero variance. Figure X.4 shows the original calculated first shell test spectrum (solid line) and the Fourier filtered EXAFS function (dotted line) using Δk: 2.3 - 19.4 $Å^{-1}$ and Δr: 1.3 - 3.1 Å. Figure X.5a shows the decrease of the variance upon shrinking the k-interval for analyses. By not using 1.0 $Å^{-1}$ at the start and 0.8 $Å^{-1}$ at the end excellent agreement is obtained between original and Fourier filtered data (k^1 variance 0.07). Using this range for fitting the Fourier filtered data leads to coordinations parameters which are nearly identical to the original values. Maximum deviations are: coordination number ±2%, Debye-Waller factor ±0.0002 $Å^2$, coordination distance ±0.003 Å, and E_0 ±0.5 eV.

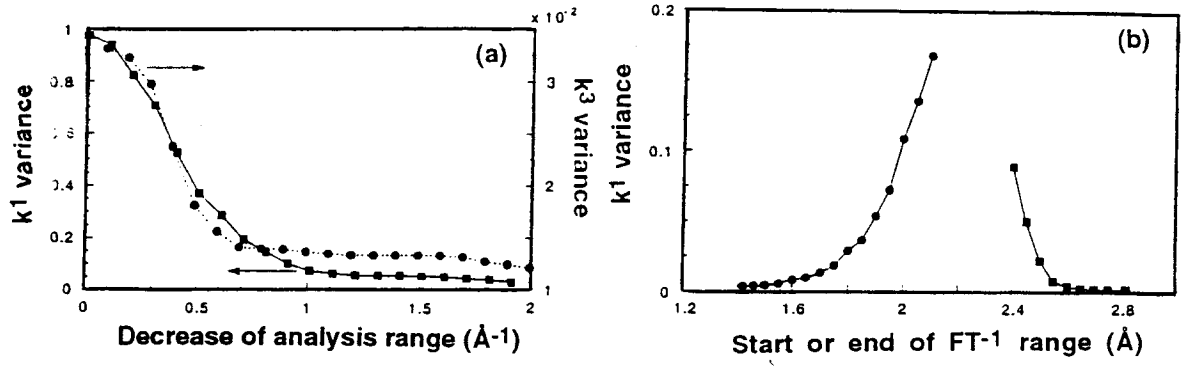

Figure X.5. — Variance of the analysis of a Fourier filtered EXAFS spectrum using its original phase shift and backscattering amplitude. a) Dependence of the variance on the analysis range in k-space. Squares: changing the start of the analysis range while keeping the end fixed at 18.5 $Å^{-1}$. Dots: changing the end of the analysis range while keeping the start fixed at 3.3 $Å^{-1}$. b) Dependence of variance for k^1 weighed analysis (from 3.5 - 18.5 $Å^{-1}$) on the inverse FT range. Dots: changing the start of the inverse FT range (keeping the end at 2.8 Å). Squares: changing the end of the inverse FT range (keeping the start at 1.3 Å).

While keeping the forward Fourier transform range at 2.3 - 19.4 $Å^{-1}$, the end and start of the inverse Fourier transform range were varied separately (see Fig. X.5b). As long as the complete main peak is included in the inverse Fourier transform excellent agreement over the complete analysis range can be obtained. Omitting only a small part of the main peak results in relatively large errors over the complete Fourier transform range. Changing the start and/or end of the forward Fourier transform range from nodes to maxima and minima does not result in a significant increase of the variance. From this it is clear that the use of special window functions is not necessary as long as the complete main peak is included in the inverse Fourier transform. Moreover, special window functions will alter the inverse Fourier transform.

X.2.5.2 Comparison of Theoretical Models

The comparisons were carried out with k^1 weighed EXAFS spectra to emphasize the differences at low k. The choice for k^1 weighed comparisons was based on the importance of the low k-region in EXAFS data analysis. Virtually all applications of EXAFS consist of measuring the XAFS of relatively heavy atoms in a matrix of low Z atoms. To determine the contribution of these low Z scatterers analysis of the heavy scatterers in the low k-region of the spectrum has to be accurate. Errors in phase or backscattering amplitude of heavy scatterers at low k will perturb the EXAFS signal at low k and thus results in unreliable results for low Z scatterers. Vaarkamp (1) et al., 1993 also carried out k^3 weighed comparisons, differences in such comparisons are much smaller and the obtained parameters more accurate. The reader is further referred to Vaarkamp (1) et al., 1993 for the details of the comparisons between the experimental first shell EXAFS functions and the model functions calculated with the different theoretical approaches. Figure X.6 shows the differences between the experimental data and the fits obtained for the different theoretical standards over the important low k data range. Numerical results are listed in Tables X.1 to X.3 for copper, rhodium, and platinum foil, respectively.

Table X.1. — Numerical results of the k^1 weighed fits of copper foil over a k-range 3.5 - 18.0 $Å^{-1}$.

Standard	N	R(Å)	$\Delta\sigma^2$ (x 10^{-3} $Å^2$)	ΔE_0 (eV)	k^1 variance
FEFF	11.01	2.542	1.66	-3.63	1.2
EXCURVE90	10.27	2.534	3.95	13.90	2.3
MUFPOT	10.00	2.527	4.16	9.27	2.6
McKale et al.	5.57	2.547	0.68	-9.38	6.2
Teo and Lee	7.73	2.499	2.20	-7.37	40.7
Input parameters for standard	12.00	2.560	σ^2 (x 10^{-3} $Å^2$) 3.28		

Table X.2. — Numerical results of the k^1 weighed fits of rhodium foil over a k-range 3.5 - 18.0 $Å^{-1}$.

Standard	N	R(Å)	$\Delta\sigma^2$ (x 10^{-3} $Å^2$)	ΔE_0 (eV)	k^1 variance
FEFF	9.19	2.698	0.17	-1.88	2.1
EXCURVE90	11.15	2.682	1.86	14.36	2.5
MUFPOT	10.57	2.671	1.84	12.36	3.2
McKale et al.	3.87	2.721	-0.84	1.71	3.5
Teo and Lee	3.59	2.691	-1.83	3.73	9.2
Input parameters for standard	12.00	2.680	σ^2 (x 10^{-3} $Å^2$) 1.40		

Table X.3. — Numerical results of the k^1 weighed fits of platinum foil over a k-range 3.5 - 18.0 $Å^{-1}$.

Standard	N	R(Å)	$\Delta\sigma^2$ (x 10^{-3} $Å^2$)	ΔE_0 (eV)	k^1 variance
FEFF	9.37	2.764	-0.72	-8.09	1.2
EXCURVE90	9.88	2.749	1.06	13.23	6.3
MUFPOT	10.17	2.739	1.30	6.00	6.1
McKale et al.	3.49	2.769	-0.76	-8.19	5.4
Teo and Lee	3.07	2.772	-2.90	-4.80	9.2
Input parameters for standard	12.00	2.774	σ^2 (x 10^{-3} $Å^2$) 2.61		

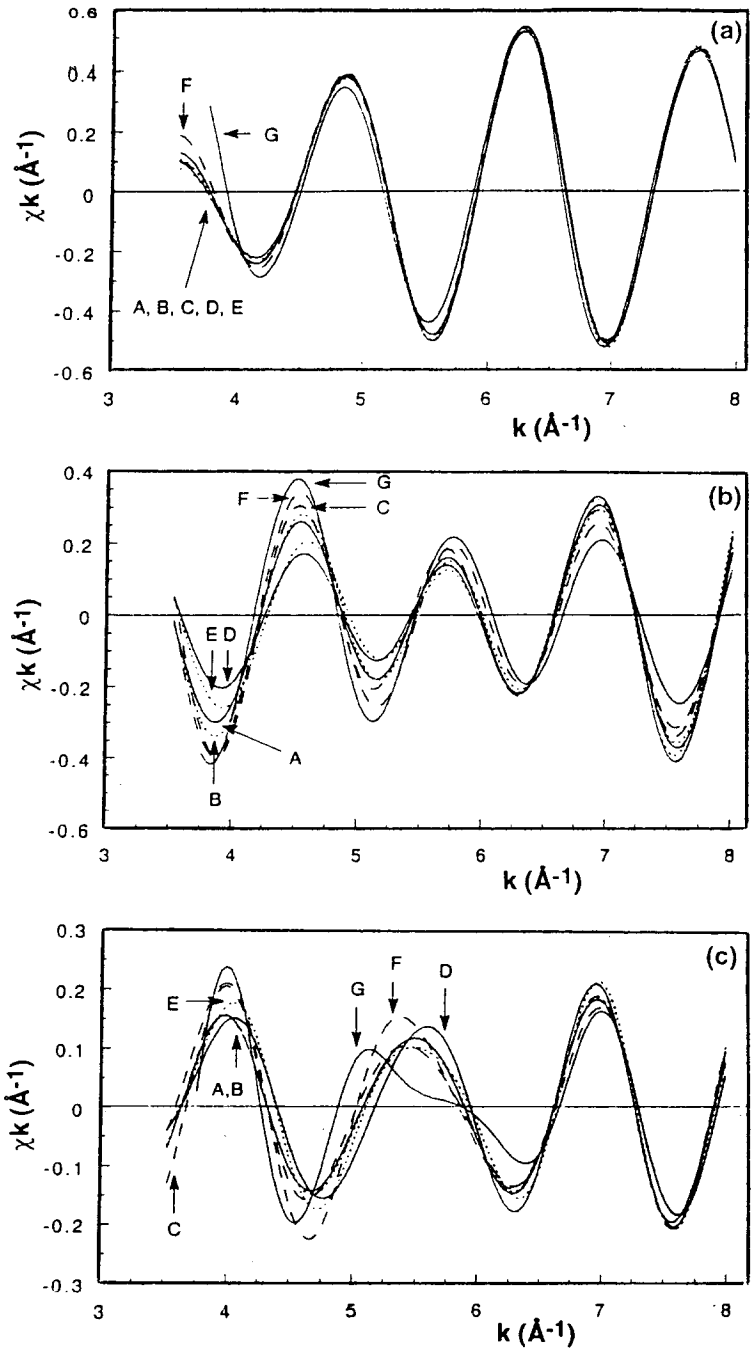

Figure X.6. — Results of analysis: a) Copper, b) Rhodium, c) Platinum. Curves: A) Experimental data, B) Experimental reference (see Vaarkamp (2), 1993), C) FEFF, D) EXCURVE90, E) MUFPOT, F) McKale et al., G) Teo and Lee.

Comparing Fig. X.6c with Fig. X.6b and X.6a leads to the conclusion that the differences between the various references are bigger for platinum than for copper or rhodium. For platinum differences in both phase and amplitude are evident below 12 $Å^{-1}$. It is important to note that for platinum only references obtained from calculations with a Hedin-Lundqvist exchange potential give acceptable fits. The

coordination numbers obtained with McKale et al. and Teo and Lee are unacceptable in all cases.

Debye-Waller factors are heavily dependent on the type of phase shift and backscattering amplitude used. Calculations with Xα exchange potentials always yield positive values. Calculations with a Hedin-Lundqvist exchange potential (FEFF), the tables of McKale et al. and the tables of Teo and Lee result in either positive or negative values with both tabulations giving large deviations in either positive or negative direction. The values for E_0 are also very dependent on the method of calculation. References calculated with a Hedin-Lundqvist exchange potential yields negative values, the Xα exchange potential gives rather large positive values, the tables of McKale et al. and the tables of Teo and Lee show inconsistent behaviour. The differences between the various codes are ascribed to the different definition of the energy zero among the theoretical standards. However, changes with element as in the tables of McKale et al. and the tables of Teo and Lee indicate an improper definition of the energy zero.

The higher variance values for heavier elements indicate that theoretical calculation of EXAFS spectra of heavy elements is not as accurate as for light elements. Analysis of EXAFS spectra with theoretically obtained phase shifts and backscattering amplitudes will result in accurate distance determinations (±0.03 Å). Other parameters vary with the type of calculation used. To obtain accurate coordination numbers a scaling factor, whose value will depend on the description of the exchange potential and the treatment of the inelastic losses, is needed. The value of this scaling factor is not transferable from one element to another. Theoretically it is expected that a scaling factor S_0^2 is required to correct the calculations for the decrease in the overlap of the passive electrons between the initial and final states of the absorbing atom. The required scaling factors to correct the coordination numbers are within the expected spread for the *ab initio* calculations. It appears that the choice of an energy dependent self-energy, as used in FEFF is the most important consideration, and that the method of potential construction is secondary, at least in monoatomic metals. The use of ground state, Xα or energy independent exchange, as in the McKale et al. tables or the codes EXCURV90 and MUFPOT is found to be inadequate and leads to large phase and amplitude errors.

The variance values found in the quantification of Fourier filtering errors (Fig. X.5) is about an order of magnitude less than the errors found in the comparison of the theoretical standards. Coordination parameters are virtually unaffected by Fourier filtering. Fourier filtering errors can be minimized by using a smaller part of the filtered EXAFS spectrum than the original. Typically the first 1.0 $Å^{-1}$ and the last 0.8 $Å^{-1}$ of the filtered EXAFS spectrum should not be used.

The reliability of the EXAFS analysis depends upon the transferability of the reference phase shift and amplitude functions. Great care must be taken in selecting the reference compounds for providing the reference amplitude and phase functions. It is of crucial importance to measure the EXAFS spectra of reference compounds at liquid nitrogen temperatures. In most cases the dynamic part of the Debye Waller factor increases strongly in going from liquid nitrogen to room temperature. The amplitude of the EXAFS spectra measured at liquid nitrogen is higher with increasing k-values (compare in Fig. X.7a solid with dotted line) which gives the opportunity to apply a forward Fourier transform over a larger range in k-space.

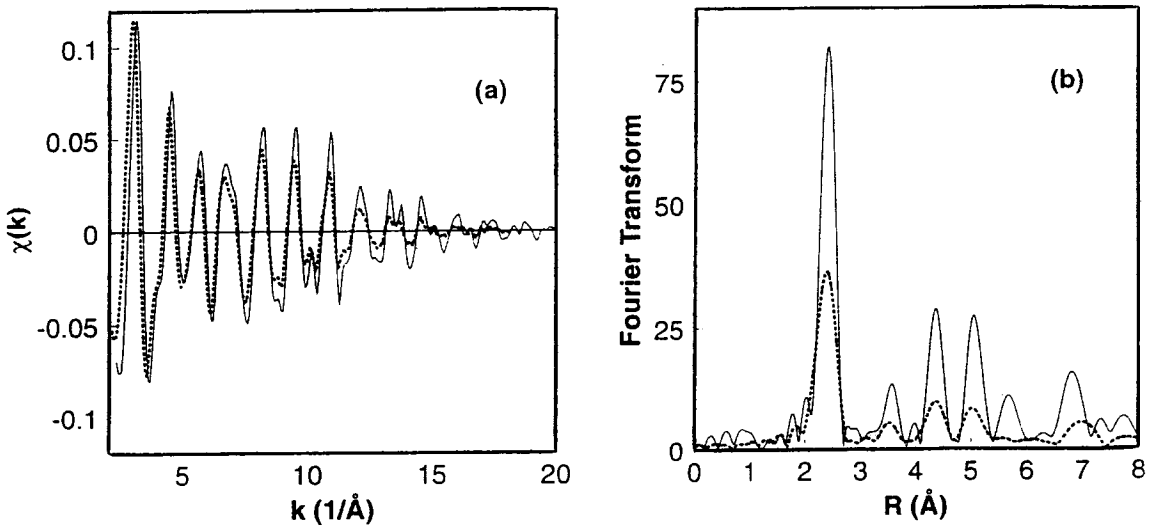

Figure X.7. — a) EXAFS spectra of rhodium foil (20 μ thickness) measured at SSRL (solid line: liquid nitrogen temperature, dotted line: room temperature). b) Fourier transform of spectra shown in a. (solid line, Δk: 2.8 - 19.4 $Å^{-1}$; dotted line, Δk: 2.6 - 15.8 $Å^{-1}$).

This leads to peaks in a Fourier transform which have a smaller width and higher amplitude (compare also in Figure X.7b solid line with dotted line). If theoretically calculated functions are used, they should be optimized by testing them on reference compounds (van Dijk et al., 1990). The accuracy of the structural parameters obtained from EXAFS analysis depends upon many factors such as the quality of the data, the length of the data range, the amount of disorder, the choice of the reference compound and the complexity of the system being studied. Typical accuracies are 1% for the determination of coordination distances, 10 to 20% for the coordination numbers and 10 to 20% for Debye-Waller factors.

X.2.6. Phase- and Amplitude Corrected Fourier Transforms. Use of Imaginary Part

As pointed out in section X.2 and shown in Fig. X.1 the phase factor $\varphi(k)$ is a non-linear function of k and the backscatterings amplitude $F(k)$ is a function of k. This implies that the Fourier transformation of an EXAFS function does not lead to an optical transform (is transform of function with constant phase and amplitude). Generally, the peaks of the Fourier transform of an EXAFS function are asymmetric. For high Z elements the k-dependence of the phase and the backscattering amplitude may even lead to the appearance of multiple peaks in the Fourier transform of an EXAFS function describing a single absorber-backscatterer pair. This have led in the past to a lot of confusion in analyzing EXAFS data containing contributions of high Z elements. A normal Fourier transform can be converted to an optical transform by removing the phase function and the backscattering amplitude. A phase- and

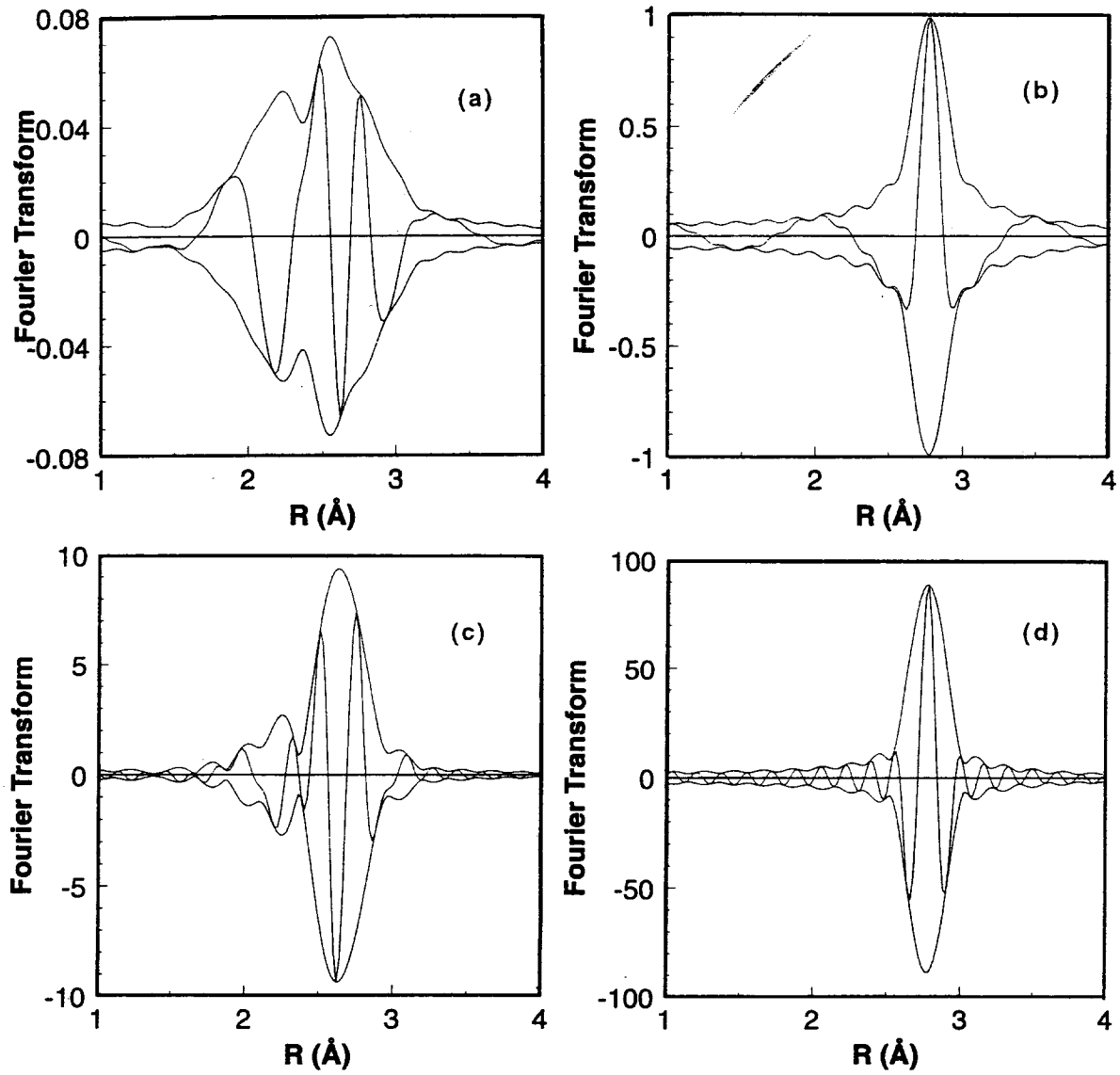

Figure X.8. — Fourier transforms with Δk: 3.1 - 18.6 Å^{-1}. a) k^1; b) k^1, Pt-Pt phase and ampl. corr.; c) k^3; d) k^3, Pt-Pt phase and ampl. corr.

amplitude corrected (optical) Fourier transform can be obtained by transformation of the following function (van Zon et al., 1985; Lytle et al., 1985):

$$\chi(k)\frac{e^{-i\varphi(k)}}{F(k)}. \qquad \text{(X.11)}$$

Figure X.8a and b shows a normal k^1 and k^3 weighted Fourier transform of a single Pt-Pt EXAFS function calculated with $N = 5$, $R = 2.77$, $\Delta\sigma^2 = 0.003$ and $\Delta E_0 = 0$. The phase shift and backscattering function were obtained from EXAFS measurements on Pt foil (thickness 4μ) measured at liquid nitrogen temperature. Since the Fourier transformation as defined in eq. X.4 is complex it is possible to calculate both the magnitude (see Fig. X.8 envelop) and the imaginary part (oscillations) of the transform. It can be seen in Fig. X.8 that the magnitude of the k^1 weighted Fourier transform of a single Pt-Pt contribution is splitted in three peaks, whereas the

imaginary part shows a complex behavior as a function of r. The applied weight factor k^n influences the k-dependence of the amplitude of the $k^n\chi(k)$ function. The magnitude of the k^3 weighted Fourier transform appears now as one asymmetric peak. Application of a phase- and amplitude corrected Fourier transform leads in all cases to a single peak with a symmetrical imaginary part, having its maximum in the top of the magnitude at the right coordination distance (see Figs. X.8c and d).

The use of optical Fourier transforms can be of great help (Kampers, 1988) in the identification of different types of neighbours by application of different phase- and/or amplitude corrections. A Fourier transform, phase- and amplitude corrected for an X-Y absorber-backscatterer pair must have a positive imaginary part peaking at the maximum of its magnitude if the EXAFS function indeed originates form an X-Y pair. Fourier transform peaks which are not symmetrical are a superposition of more than one contribution.

X.2.7. Detection of Low Z Scatterers

It is tempting to apply a k^2 or k^3 weighting to the EXAFS spectrum during the fitting in k-space to compensate for the decay in amplitude of the spectrum with k. Also Fourier transformation of a function which has an equalized amplitude results in less broadened peaks, which are easier to filter for inverse transformation. However, applying a k^2 or k^3 emphasizes the high Z contributions to the spectrum since high Z elements have more scattering power at high values of k than low Z elements. As pointed out in section X.2.1 low Z elements have the highest amplitude at low values of k. Therefore, the use of a k^2 or k^3 weighted EXAFS spectrum or Fourier transform makes the analysis much less sensitive for the presence of low Z contributions in the EXAFS data. This is demonstrated in Fig. X.9. Pt-Pt and Pt-O EXAFS model functions have been calculated with the coordination parameters as given in Table X.4. These parameters are in the range of typical parameters found in the EXAFS analyses of data collected on small metal particles dispersed on high surface area supports. Pt-Pt and Pt-O phase shift functions and Pt and O backscattering amplitudes have been obtained from EXAFS data collected from Pt-foil and $Na_2Pt(OH)_6$, which were measured at liquid nitrogen temperature. Figure X.9a shows the individual Pt-Pt (solid line) and Pt-O (dotted line) EXAFS spectra calculated with the parameters of Table X.4. The sum of the Pt-Pt and Pt-O EXAFS functions is also plotted (dashed line) and this function mimics the experimental data. The difference between the EXAFS spectrum with only a platinum contribution and the EXAFS spectrum with a platinum and an oxygen contribution is most pronounced below 6 $Å^{-1}$. In the k^3 weighted Fourier transform of the spectra (shown in Fig. X.9c) the difference between the spectrum with only a platinum contribution and the simulated experimental EXAFS spectrum (with a platinum and an oxygen contribution) is hardly detectable. The k^1 weighted Fourier transform (Fig. X.9b)

Table X.4. — Parameters used in the calculation of the model spectra.

Coordination	N	R(Å)	$\Delta\sigma^2$ ($Å^2$)	ΔE_0 (eV)
Pt-Pt	5.0	2.77	0.003	0
Pt-O	1.9	2.65	0.006	0

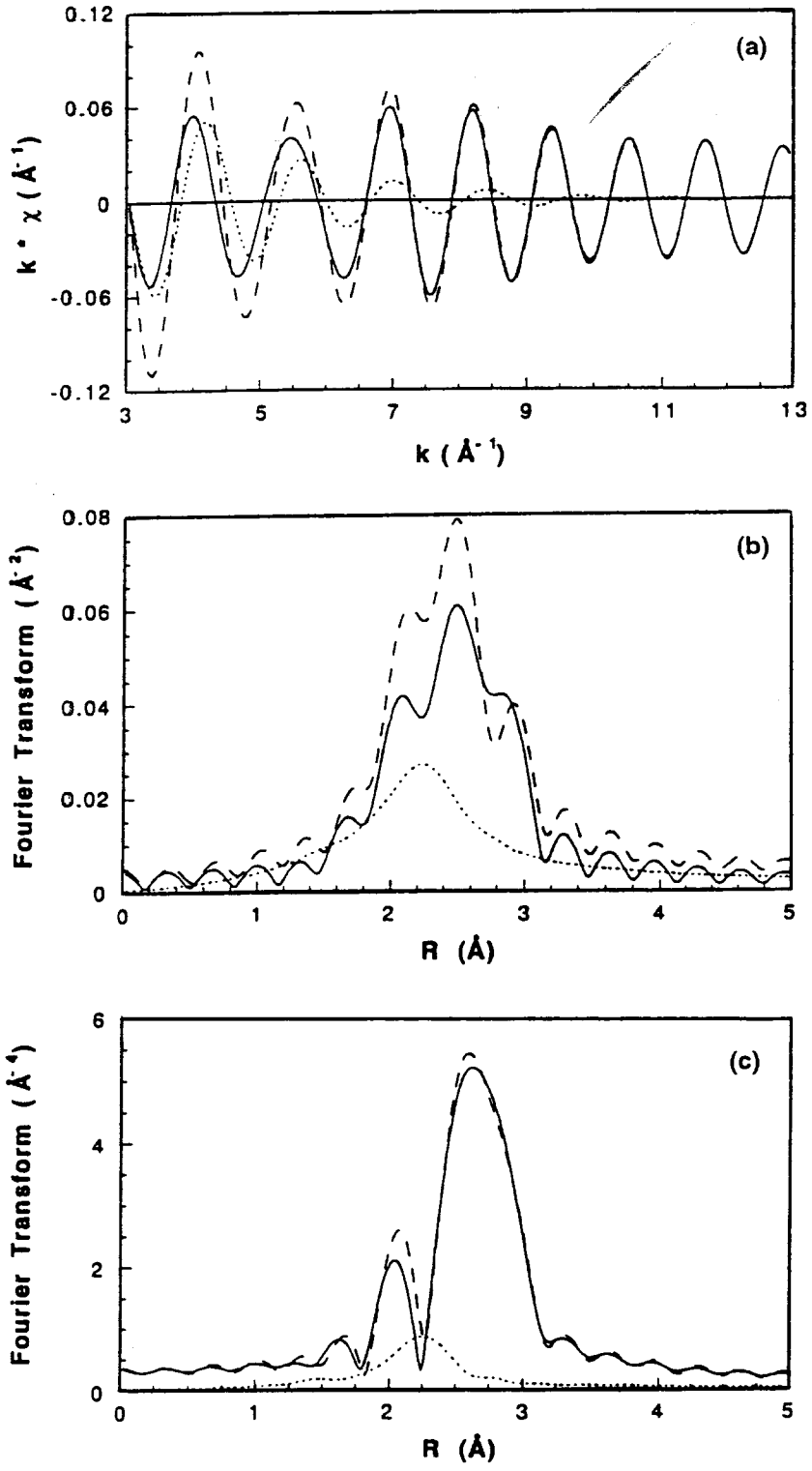

Figure X.9. — Simulated EXAFS spectra of Pt-Pt (solid line), Pt-O (dotted line) and Pt-Pt + Pt-O (dashed line). a) EXAFS functions, b) k^1 weighed Fourier transform (Δk: 3.5 - 13.0 $Å^{-1}$), c) k^3 weighed Fourier transform (Δk: 3.5 - 13.0 $Å^{-1}$).

shows much larger differences. From this model study it is obvious that for a proper analysis of low Z contributions present in EXAFS spectra k^1 weighted fits and/or Fourier transforms should be applied.

X.2.8. Correlation Between N and $\Delta\sigma^2$. Use of Both k^1 and k^3 Weighted Fourier Transforms

The determination of a unique set coordination parameters for a particular contribution to an EXAFS spectrum is often difficult due to the correlation between the value of the coordination number N and the Debye-Waller factor $\Delta\sigma^2$. Kampers, 1988 showed that by simultaneous minimization of the difference between fit and data in a k^1 and k^3 weighted Fourier transform, a unique set of parameters can be found. This can be rationalized by examining eq. X.2 and noting that the amplitude of the EXAFS spectrum depends on both N and $\Delta\sigma^2$. More particularly, different combinations of N and $\Delta\sigma^2$ will lead to the same peak amplitude of the Fourier transform of an EXAFS spectrum. However, this set of combinations depends on the weight factor, which has been used for the Fourier transform. The combination of N and $\Delta\sigma^2$ that gives a good fit both in a k^1 and k^3 weighted Fourier transform offers a unique set of parameters. An example of this approach is given in Fig. X.10. Figure X.11b displays the k^3 weighed Pt-Pt phase- and amplitude corrected Fourier transforms of three EXAFS spectra calculated with the combinations of N and $\Delta\sigma^2$, which compose the k^3 curve of Fig. X.10. At the onset of the main peak some differences are present, but the amplitude of the main peak of the transform of these spectra is equal. However, the k^1 weighed Pt-Pt phase- and amplitude corrected Fourier transforms of the same three EXAFS spectra (Fig. X.11a) are very different. Only if Fourier transforms with both k^1 and k^3 weighting show good agreement between model and experimental data a "good" combination of coordination number and Debye-Waller factor has been selected. It is essential to use phase- and

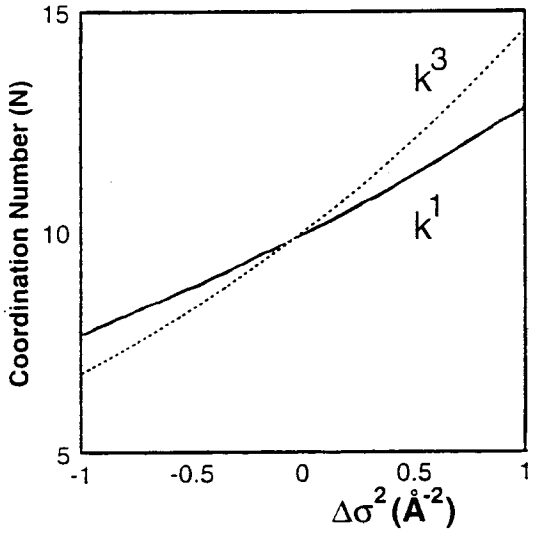

Figure X.10. — Combinations of coordination number (N) and Debye-Waller factor ($\Delta\sigma^2$) giving good fits in k^1 or k^3 Fourier transform.

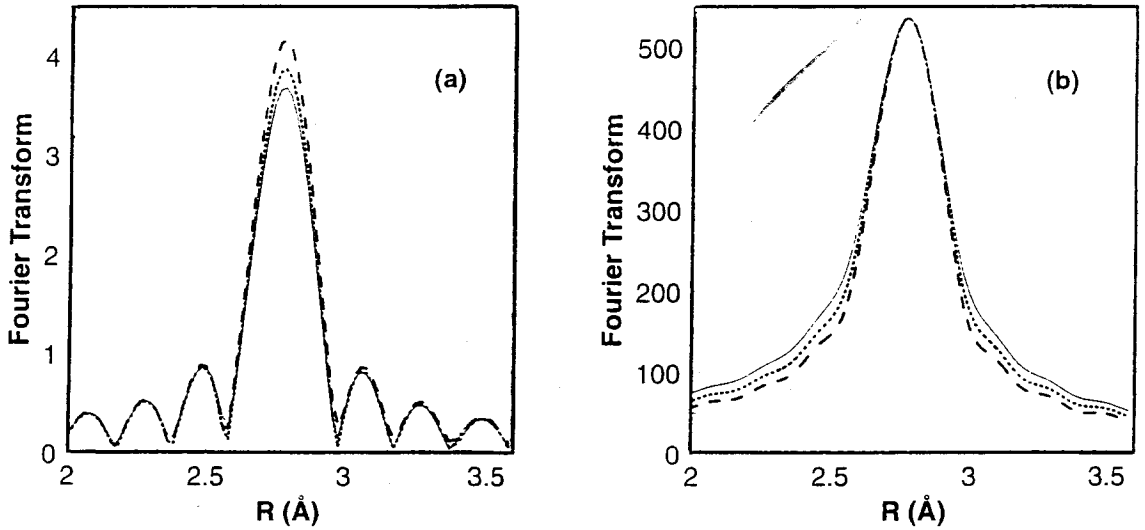

Figure X.11. — Fourier transforms (Δk: 3.1 - 18.6; Pt-Pt phase and amplitude corr.) of EXAFS model functions. Solid line: N=8.2, $\Delta\sigma^2$= -0.0005 Å^2; Dotted line: N=10, $\Delta\sigma^2$= 0 Å^2; Dashed line: N=12.3, $\Delta\sigma^2$= 0.0005 Å^2. a) k^1 weighed, b) k^3 weighed.

amplitude corrected Fourier transforms when applying this method, because otherwise the asymmetry of the peaks will obscure the results.

X.3. Stereo Chemistry: Metal-Support Interaction of Small Iridium Clusters Dispersed on MgO (An Example of the Uniqueness of EXAFS Spectroscopy)

X.3.1. Introduction

Most industrial metal catalysts are dispersed as small particles on high-area metal oxide supports to allow access of reactants to most of the metal atoms. The dispersion is stabilized by metal-support interactions that hinder particle migration and coalescence that lead to loss of catalytic activity by loss of metal surface area. Metal-support interactions also affect the activities of catalysts, but little is understood about how (Stevenson et al., 1987; Haller et al., 1989). The understanding is limited by the lack of precise methods for structural characterization of microscopic metal particles and metal-support interfaces. Van Zon et al., 1993 have shown that small, uniform supported metal clusters offer an excellent opportunity for precise characterization of the structure of the metal clusters and the metal-support interface by EXAFS spectroscopy; the smaller the metal cluster, the larger the fraction of the EXAFS signal that arises from the metal-support interface and the greater the opportunity for accurate characterization of the interface structure. The $[Ir_4(CO)_{12}]$ metal carbonyl cluster was chosen to be the precursor, and partially hydroxylated MgO was chosen to be the support, as the chemistry of Ir carbonyls on the basic MgO surface is relatively well understood (Maloney et al., 1990) being similar to that occurring in basic solutions and allowing synthesis in high yields of $[HIr_4(CO)_{11}]^-$ on the surface (Maloney et al., 1991). The goal was to form and decarbonylate this cluster anion on the support without changing its nuclearity. The MgO support offers several advantages for characterization of the samples by X-ray

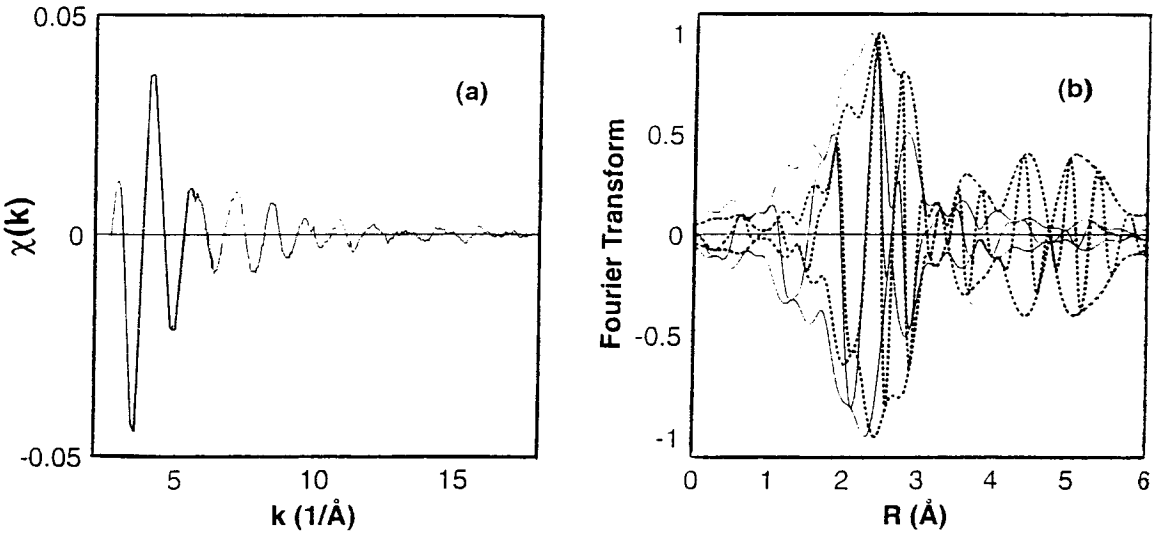

Figure X.12. — a) Raw EXAFS data of Ir_4/MgO. b) Normalized Fourier transforms (k^1, Δk: 2.6 - 13.5 $Å^{-1}$) of Ir_4/MgO (solid line) and Ir powder (dotted line).

absorption spectroscopy. In contrast to the structurally more complex γ-Al_2O_3 and TiO_2, MgO (which has the rock salt structure) exhibits predominantly (100) faces, even in the powder form (Henrich, 1985). Thus the surface of MgO is relatively simple and well defined and a good choice for characterization of the metal-support interface. Furthermore, as both the O^{2-} and Mg^{2+} ions are present in the same surface layers, both the Ir-O and Ir-Mg interactions are expected to be characterized by the EXAFS data. EXAFS evidence of interactions between supported metals and cations of the support has been reported only rarely (Koningsberger et al., 1992).

Table X.5. — Coordination parameters obtained from fitting the Ir_4/MgO EXAFS spectrum.

Parameters	N	R(Å)	$\Delta\sigma^2 \times 10^{-3}$ ($Å^2$)	ΔE_0 (eV)
Coordination:				
Ir-Ir	2.6 ± 0.3	2.713 ± 0.004	0.6 ± 0.7	-5.2 ± 0.7
Ir-O	3.4 ± 0.1	2.63 ± 0.01	3.8 ± 0.7	-0.8 ± 0.6
Ir-Mg	0.3 ± 0.1	1.60 ± 0.02	13.6 ± 4.3	-2 ± 4

X.3.2. Results

The sample designated Ir_4/MgO represents that prepared by decarbonylation of $[HIr_4(CO)_{11}]^-$ supported on MgO. The raw EXAFS data characterizing Ir_4/MgO is shown in Figure X.12a. The data quality is high. A preliminary indication of the Ir cluster size is given by the Fourier transforms of Figure X.12b, which is a comparison of a k^1-weighted Fourier transform of data characterizing Ir powder and data characterizing the Ir_4/MgO sample. The Fourier transform of the EXAFS data characterizing the Ir powder in this figure is scaled to the main peak of the Fourier transform of the EXAFS data characterizing Ir_4/MgO. Figure X.12b shows both the magnitude (the envelope) and the imaginary part (the oscillations) of the k^1-weighted Fourier transform. It can be seen that the second, third, and fourth Ir-Ir

shells are not detectable in the Ir_4/MgO sample. The presence of low-Z neighbors of Ir is also demonstrated in Figure X.12b. The peak at the position of the first Ir-Ir shell in Ir powder seems to be split into three peaks; this splitting is caused by the *k* dependence of the phase shift and backscattering amplitude of the Ir-Ir absorber-backscatterer pair (see also section X.2.6). The contrast between the data in the first-shell region for the two samples (Fig. X.12b), both the magnitudes and the imaginary parts of the Fourier transforms) demonstrates the presence of low-Z scatterers in the immediate neighborhood of Ir in the Ir_4/MgO sample; these are inferred to be present in the metal-support interface.

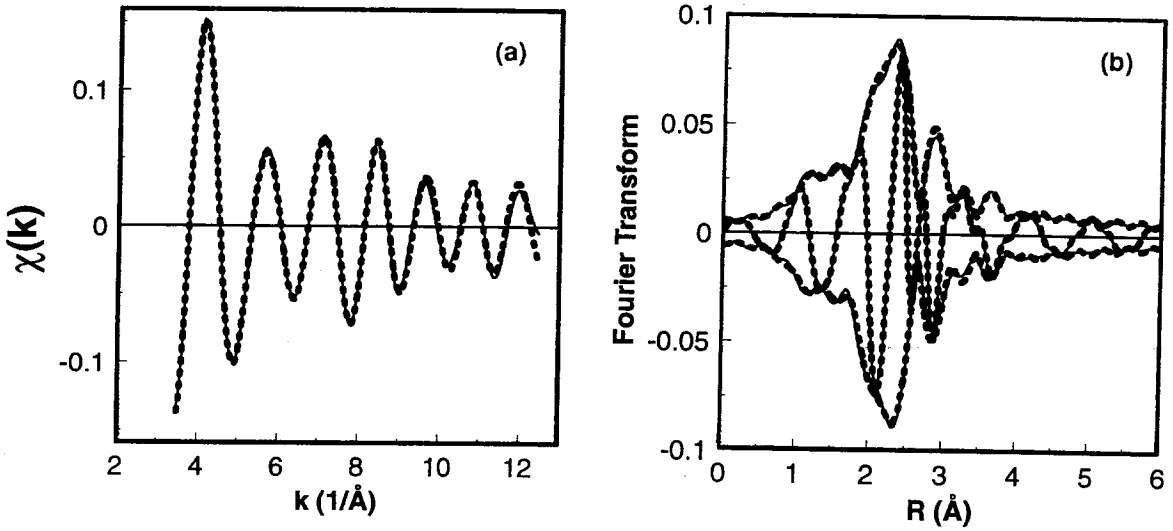

Figure X.13. — Results of multiple shell fitting (dotted line) of the EXAFS data characterizing Ir_4/MgO (solid line). a) Fit in k-space (k^1, Δk: 3.5 - 12.5 $Å^{-1}$) and b) fit in R-space (FT: k^1, Δk: 3.5 - 12.5 $Å^{-1}$).

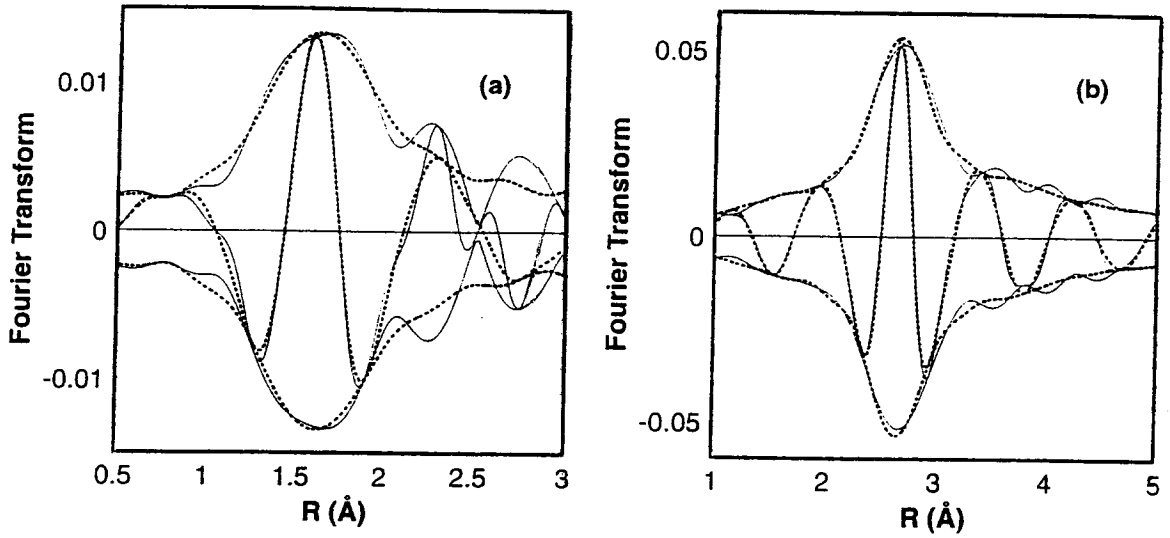

Figure X.14. — a) Fourier transform (k^3, Δk: 3.5 - 12.5 $Å^{-1}$, Ir-Mg phase corrected) of difference file (isolated EXAFS minus calculated Ir-Ir + Ir-O) (solid line) and calculated Ir-Mg EXAFS function (dotted line). b) Fourier transform (k^3, Δk: 3.5 - 12.5 $Å^{-1}$, Ir-O phase corrected) of difference file (isolated EXAFS minus calculated Ir-Ir + Ir-Mg) (solid line) and calculated Ir-O EXAFS function (dotted line).

The final results of the EXAFS data analysis is presented in Figure X.13. Fits obtained by a nonlinear least squares multiple-shell fitting routine are shown in k space and in r space with k^1 weighting. The coordination parameters and their standard deviations (calculated from the covariance matrix including the statistical multiple-shell fitting routine), are given in Table X.5. The Ir-O and Ir-Mg errors of the experimental points, obtained from the nonlinear least squares contributions are evidence of the metal-support interactions. These contributions are shown for the Ir_4/MgO sample in Figure X.14a and b. The Ir-O EXAFS function was determined by subtraction of the calculated sum of the (Ir-Ir) + (Ir-Mg) contributions from the primary EXAFS data by using the coordination parameters obtained from the best fit. Similarly, the Ir-Mg EXAFS function was obtained by subtraction of the calculated (Ir-Ir) + (Ir-O) contribution from the primary data. The Ir-O phase-corrected Fourier transform peaks at about 2.6 Å, and the Ir-Mg phase-corrected Fourier transform peaks at about 1.6 Å. More details of this analysis are given by van Zon et al., 1993. In particular, the authors discuss in detail the statistical significance of the Ir-O and Ir-Mg contributions.

X.3.3. Discussion

A unique advantage of the organometallic precursors is the opportunity they offer for preparation of extremely small supported metal clusters that are almost optimally suited to precise characterization with EXAFS spectroscopy. The results of the work of van Zon et al., 1993 give evidence that the tetrairidium cluster can be decarbonylated on the support with little change in nuclearity (Table X.5). Since the clusters are so small, the EXAFS signal is determined in large measure by the metal-support interactions and not just the metal-metal interactions. Consequently, the EXAFS data offer the prospect of detailed characterization of the structure of the metal-support interface.

The Ir-Ir coordination number of 2.6 is consistent with the inference that the cluster nuclearity was maintained. However, within the experimental error

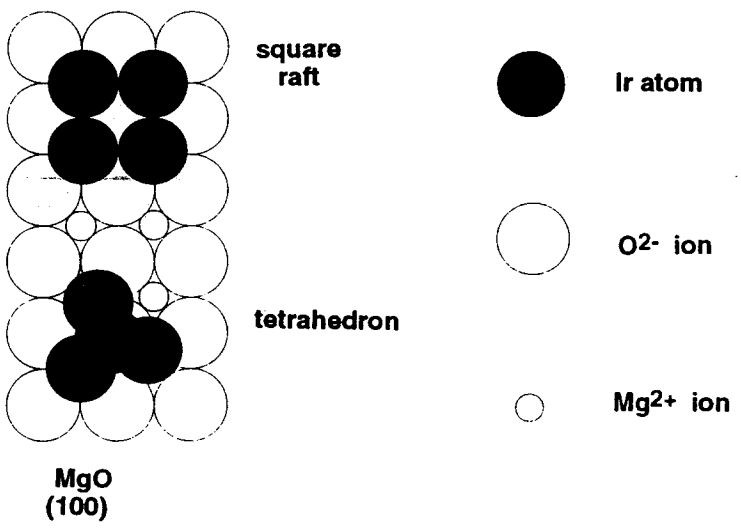

Figure X.15. — Structural model of Ir_4/MgO based on the EXAFS data. The MgO (100) surface is assumed.

(Table X.5), this value is less than 3.0, the value characteristic of the tetrahedron of the metal frame of the precursor $[Ir_4(CO)_{12}]$ or $[HIr_4(CO)_{11}]^-$, which implies that the tetrahedral frame of the precursor was not retained in all the clusters. The average Ir-Ir coordination number of 2.6 cannot be reconciled with raft-like structures alone either, as the first-shell Ir-Ir coordination number in a square Ir_4 raft is 2, and much larger rafts must be assumed to account for N = 2.6 (but these imply sizeable third and fourth Ir-Ir shells). A small fraction of clusters with nuclearities greater than four may have been present; however, as the third and fourth Ir-Ir shells are almost absent, these must have been rare. There is no conclusive evidence that raft-like structures would be exclusively square; various other arrangements can not be ruled out. The EXAFS data have been modeled as simple as possible; they have been found to be consistent with a mixture of Ir_4 tetrahedra and square rafts (see Fig. X.15). Taking the accuracy of their analysis results, the authors infer that 40-50% of the Ir clusters are tetrahedra and the remainder square rafts.

The Ir-O and Ir-Mg contributions are pronounced in the EXAFS data. These contributions are attributed to the metal-support interface. The actual interfacial iridium-oxygen coordination number for the Ir_4/MgO sample can be calculated directly from the coordination number determined for the Ir-O shell (3.4) using the earlier mentioned estimated fraction of iridium clusters present as a tetrahedron on the MgO (100) surface (0.5). In the tetrahedron 75%, and in the raft 100% of the iridium atoms are present in the metal-support interface. This leads to the following equation: $(0.5 * 0.75 * N(i))_{tet} + (0.5 * 1 * N(i))_{raft} = 3.4$, resulting in $N(i) = 3.9$. Taking into account the experimental errors in the EXAFS data (Table X.5), we might

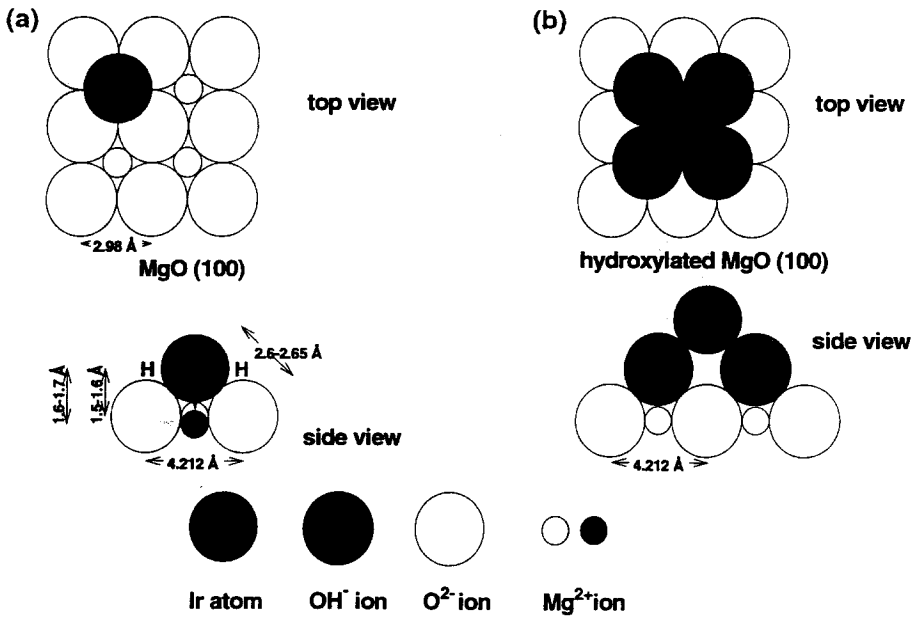

Figure X.16. — Structural models of the Ir_4/MgO interface. A) Ir metal atom on a partially hydroxylated MgO (100) surface with hydrogen in the metal-oxygen interface. B) Ir metal atom on a fully hydroxylated MgO (100) surface.

therefore suggest that the Ir-MgO interface could be modeled with an Ir-O coordination number of four; a fourfold Ir-O coordination can be visualized on the (100) face of MgO. This is the predominant face (Henrich, 1985).

The EXAFS observations raise fundamental questions about the nature of the interactions at metal-support interfaces. Van Zon et al., 1993 discuss extensively the suggestions that the long metal-oxygen distances (2.6-2.8 Å) observed in this work and for numerous other samples (Koningsberger et al., 1992) may indicate the presence of hydrogen in the metal-support interface or, alternatively, interactions of metal atoms with hydroxyl groups of the surface (Koningsberger et al., 1992). As outlined above, the Ir at the interface is inferred to be coordinated principally to four oxygens. The oxygens on the surface of partially hydroxylated MgO include O^{2-} as well as oxygen of OH^- groups of more than one kind, including protonated O^{2-} ions terminating the MgO lattice and OH groups bonded to Mg^{2+} ions terminating the lattice (Lamb et al., 1988). This results in two limiting cases for the Ir atoms at the MgO surface (Fig. X.16).

The two simple models can be described as follows: (1) If the support surface has no hydroxyl groups in contact with the clusters, individual Ir atoms on the MgO (100) face are positioned between the oxygens and directly above the Mg^{2+} ions (Fig. X.16a). From the MgO crystallographic distance (Henrich, 1985) and an Ir-O coordination distance of 2.6 Å (Table X.5), an Ir-Mg distance of 1.5-1.6 Å is expected. (2) If the MgO (100) face is fully hydroxylated, then the Mg^{2+} ions are covered with OH groups. Ir atoms on this surface that have an Ir-O coordination number of four would have to be placed between four OH groups, each positioned on top of a Mg^{2+} surface ion (Fig. X.16b). Using the same coordination distances as in the former model and a Mg-OH distance of 2.106 Å (equal to the Mg-O distance in MgO), an Ir-Mg distance of 4.1-4.2 Å is calculated. The Ir-Mg distances indicated by EXAFS (1.6-1.7 Å, Table X.5) are in agreement with the first but not the second of these limiting-case models.

X.4. Determination of The Electronic Structure: White Line Intensities of L_{II} and L_{III} Edges as Probe for the d-Band Density of States of Transition Metals (XANES)

X.4.1. Introduction

In the following sections a very fundamental issue in catalysis by metals has been addressed. The intrinsic metal properties leading to very important catalytic applications can be changed by interaction with the support or by adding so-called promotor ions. Catalytic and modern spectroscopy studies strongly suggest that catalytic properties like activity and selectivity can be modified by charge transfer or polarization at the interface between very small metal particles and the support or the promoting ions (Boudart et al., 1984).

Information about the d-band density of states in transition metal clusters can be obtained from the white line intensities of the L_{II} (transition from $2p_{1/2}$ to $5d_{3/2}$) and L_{III} (transition from $2p_{3/2}$ to $5d_{5/2}$ and $5d_{3/2}$) X-ray absorption edges. A basic theory of white lines has been given by Mott, 1949; Brown et al., 1977 and Mattheiss et al., 1980. The theoretical calculations of the unoccupied Pt d-states show that the J=5/2 final state is predominant. Brown et al. showed that the J=5/2 states contribute

about 14 times more to the final d-states than the J=3/2 states. Mattheis et al. calculated that the ratio of the unoccupied states ($h_{5/2}/h_{3/2}$)ranges from 3.5 within 0.5 eV of the Fermi level to 2.9 over the entire unoccupied conduction band. These calculations explain why the intensity of the white line of the L_{III} X-ray absorption edge is much higher than the intensity of the L_{II} edge in bulk platinum.

Several authors have used the L_{III} X-ray absorption edge spectra to characterize the chemical state of the absorbing atom in transition metal compounds. Lytle et al., 1976 and 1979 have shown for iridium, platinum, and gold that the intensity of the white line of the L_{III} X-ray absorption edge is proportional to the d-electron vacancies. Samant et al., 1991 reported a decrease in the intensity of the L_{III} X-ray absorption edge of platinum upon removal of hydrogen from the surface for measurements carried out at low temperature, whereas Lytle (2) et al., 1985 reported a slight intensity increase of the L_{III} edge upon hydrogen removal. However, a decrease in intensity of the L_{II} edge upon hydrogen removal was shown. The important consequence of this observation is that both the L_{III} and the L_{II} edge have to be examined before any statement about a change in electron density can be made.

From the factors influencing the white line intensity the particle size and the support are of course of most interest in catalysis. The relation between LDOS and particle size is of interest as this might explain the particle size sensitivity of some reactions. The establishment of the effect of the support on the LDOS is expected to give a physical key to the changes in reactivity of small metal clusters on different supports or in the presence of different cations.

Gallezot et al., 1977 and 1979 reported that the white line intensity of the L_{III} edge of 1-nm Pt clusters in Pt/NaY is larger than 3-nm clusters. Mansour et al., 1984 carried out a more quantitative study including the white line of the L_{II} absorption edge for Pt/SiO_2 with an average particle size of 15 Å (72 atoms) and determined that there were 14% more d-holes than in bulk platinum metal. An increase in the d-band density of states of surface atoms due to the decreased degree of delocalization has been discussed by Gordon et al., 1977 and Saillard et al., 1984. A recent theoretical study, using local-density methods on neutral and charged Ir_4 and Ir_{10} clusters (Ravenek et al., 1989) indicates a higher number of d-electrons for the Ir_4 cluster in comparison to the Ir_{10} cluster. However, introduction of a core hole, to mimic the X-ray absorption process, into the clusters results in a lower number of d-electrons for the Ir_4^+ compared to the Ir_{10}^+ cluster. The higher electron deficiency for the smaller cluster is due to a less efficient screening of the core hole.

Changes in the intensity of the L_{III} X-ray absorption edge of a Pt/SiO_2 catalyst have been related to alterations in the d-band density of states resulting from a change in metal-support interaction after reduction at high temperatures (Lytle (2) et al., 1985. Gallezot et al., 1977 and 1979 reported that platinum clusters in Ce-promoted NaY zeolite have a larger number of holes in the d-band than platinum in NaY zeolite. Recently, the number of unfilled d-states of platinum particles supported on silica were reported to become more electron deficient loading the sample with increasing amounts of Na (Yoshitaka et al., 1991).

The recent results obtained by Vaarkamp (2), 1993 will be discussed in the following. He has shown that chemisorbed hydrogen is a first order effect on the d-band density of states of small metal particles. The important outcome of his study is that X-ray absorption data have to be taken under vacuum before any conclusion

can be drawn about changes in the d-band density of states due to support or promotor effects.

X.4.2. Experimental

A 1.0 wt% $Pt/\gamma\text{-}Al_2O_3$ catalyst was prepared by impregnation of Ketjen CK-300 (200 m^2/g, 0.6 cm^3/g) with an aqueous solution of hydrochloric platinic acid. The catalyst was dried in air overnight at 120°C before it was reduced at 450°C for 4 hours. After reduction the catalyst was passivated at room temperature (further details of the preparation procedure are given by Vaarkamp (2) et al., 1993).

The X-ray absorption data were obtained at the Synchrotron Radiation Source in Daresbury, U. K., Wiggler Station 9.2 in the transmission mode at liquid nitrogen temperature. The estimated resolution at the Pt L_{III} (11564 eV) and L_{II} (13273 eV) edge is 3 eV. The Si(220) monochromator was detuned to 50% intensity to avoid the effects of higher harmonics. In order to obtain an absolute energy calibration of the data a third ion chamber was used with a platinum metal foil (thickness 4 μ) placed between the second and the third ion chamber. Each spectrum was separately calibrated at the L_{III} and L_{II} edge. The spectra were normalized by the edge jump at 50 eV above the edge. Self-supporting wafers ($\mu x = 2.5$) were reduced in flowing H_2 in an *in-situ* cell (Kampers et al., 1989). The $Pt/\gamma\text{-}Al_2O_3$ sample was rereduced at 300 (LTR) and 450°C (HTR). After collecting the data on the reduced catalyst the cell was evacuated to 10^{-5} Torr at RT and heated to the evacuation temperature. Maintaining the vacuum, the cell was held at the evacuation temperature for an additional hour and cooled to RT. After collecting the data on the evacuated catalyst, hydrogen was admitted into the cell at RT. Subsequently the sample was heated to 200°C under flowing hydrogen and held there for one hour. Data on the reduced samples were obtained in the presence of H_2, data on the evacuated samples were obtained under dynamic vacuum.

X.4.3. Results

X.4.3.1. Structural characterization

Characterizations of the catalyst by H_2 TPD, hydrogen chemisorption, and EXAFS are reported by Miller et al., 1993 and Vaarkamp (3) et al., 1993. The structure of the metal-support interface changes with reduction temperature. After LTR a Pt-O contribution at a distance of 2.7 Å is present in the EXAFS spectrum. Based on hydrogen TPD this long Pt-O distance has been attributed to a structure were atomic hydrogen is present between the platinum and the oxygen atoms of the support. Treatment in either inert or hydrogen atmosphere at high temperature removes this interfacial hydrogen. Hence, the Pt-O distance, as determined by EXAFS, is shortened to 2.2 Å. The EXAFS first-shell coordination numbers, which are important for an evaluation of the white line results are given in the Table X.6.

X.4.3.2. White line intensity determination

The measured Pt L_{II} and L_{III} X-ray absorption edges are a combination of a smooth function representing the transition of electrons from core-levels into the continuum and a function representing the transition of core-level electrons into

unfilled states in the valence band. Hence, to evaluate the number of unfilled states these two functions have to be separated. Horsley, 1982 showed that the Pt L_{III} edge of platinum foil can be deconvoluted in a smooth arctangent function and a Lorentz function representing atoms transferred to the Pt 5d level (Fig. X.17a). However, this deconvolution of the edge is unable to cope with the asymmetric form of the X-ray absorption edge of the supported platinum catalysts when hydrogen is chemisorbed on the surface. A representative example of this deconvolution for a Pt/K-LTL sample reduced at 300°C is shown in Figure X.17b. It is clear that the fitted Lorentz function is not representative of the area of the white line of Pt/K-LTL, hence an alternative approach is needed. Vaarkamp (2), 1993 checked whether the white line consists of more than one Lorentz function by calculating the second derivative of the spectrum, thereby diminishing the contribution of the smooth background (Lytle et al., 1990). Only one negative peak was present indicating that the white line consists of a single transition. To quantify the differences in white line intensity between the catalysts and platinum foil the approach described by Mansour et al., 1984 was used.

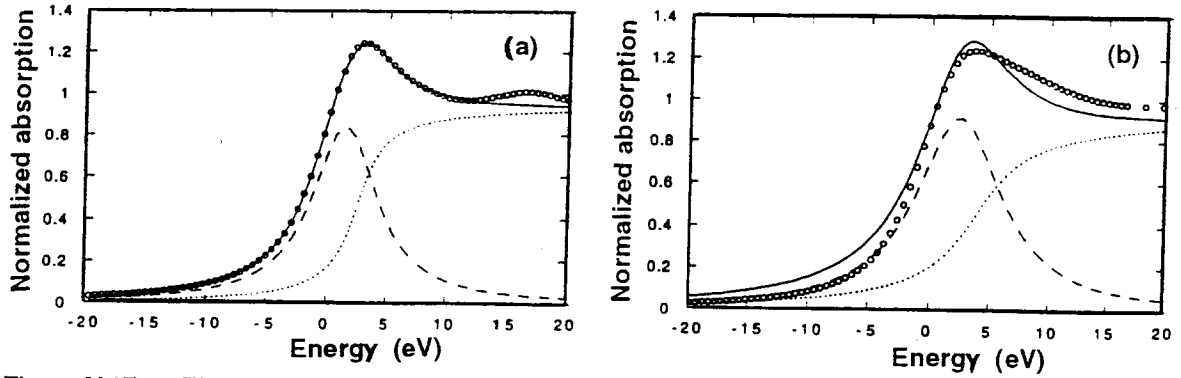

Figure X.17. — The Pt L_{III} edge (circles) of a) platinum foil and b) Pt/K-LTL reduced at 300°C with an arctangent (dotted line) and Lorentz (dashed line) obtained by non linear fitting, solid line: sum of arctangent and Lorentz.

The normalized XAFS spectra of the Pt L_{II} and L_{III} edge of the platinum foil and the catalyst were aligned at there inflection points. After subtraction of the platinum foil data from the data of the catalyst, the resulting curves were numerically

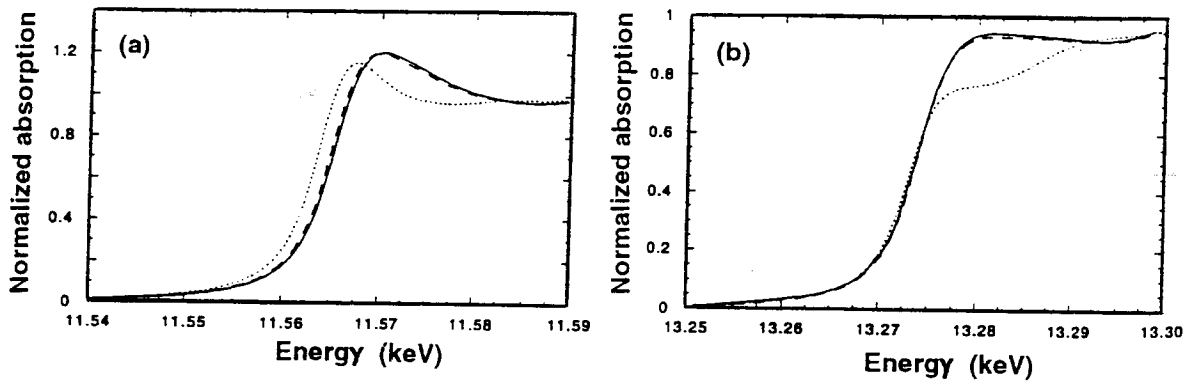

Figure X.18. — X-ray absorption edge of Pt/γ-Al_2O_3 after reduction at 300°C (solid line), subsequent evacuation at 300°C (dotted line) and subsequent admission of hydrogen at 200°C (dashed line). a) L_{III} edge and b) L_{II} edge.

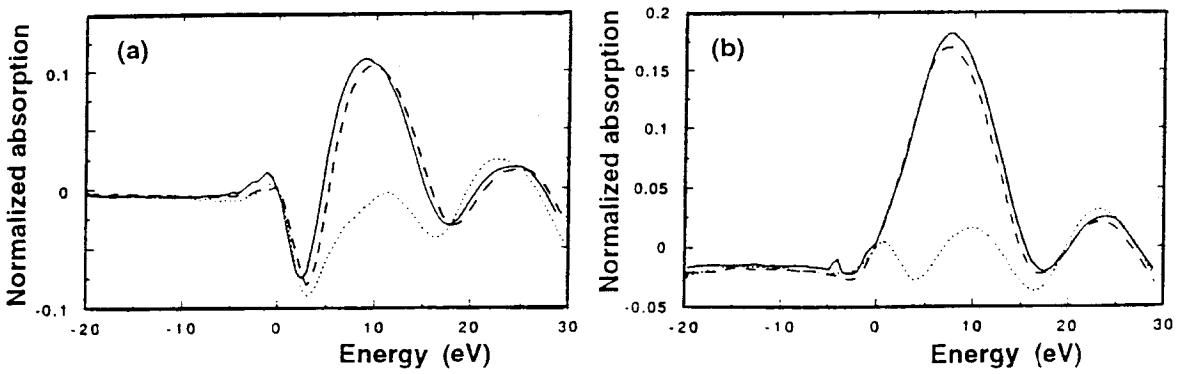

Figure X.19. — Difference between the X-ray absorption edges of $Pt/\gamma\text{-}Al_2O_3$ and the corresponding edge of platinum foil after reduction at 300°C (solid line), subsequent evacuation at 300°C (dotted line) and subsequent readmission of hydrogen at 200°C (dashed line). a) L_{III} and b) L_{II} edge.

integrated between -2 and +17 eV for both the L_{III} (ΔA_3) and the L_{II} (ΔA_2) edge. The resulting areas were combined to give the difference in the total number of unfilled states in the d-band (Δh_T) (Mansour et al., 1984) in comparison to bulk platinum:

$$\Delta h_T = 2.25\ (\Delta A_3 + 1.11\ \Delta A_2) \qquad (X.11)$$

A change in h_T of 7 (which is approximately the largest change observed in this study) corresponds to 0.08 electron per atom. The alignment of the X-ray absorption edge of platinum foil and the catalyst has a dramatic effect on the difference spectrum of the platinum foil and the catalyst (Mansour et al., 1984). To circumvent the problem of the changing edge position by an increase in white line intensity one should align the smooth background function in the edges of interest. The position of the smooth background function can be deduced from the position of the EXAFS wiggles. However, in the samples which were studied by Vaarkamp (2), 1993 the EXAFS wiggles are subject to change. Consequently a systematic alignment procedure based on the EXAFS wiggles is not possible. To ensure a systematic approach for the determination A_3 and A_2 Vaarkamp (2), 1993 aligned the inflection points of the platinum foil and the sample.

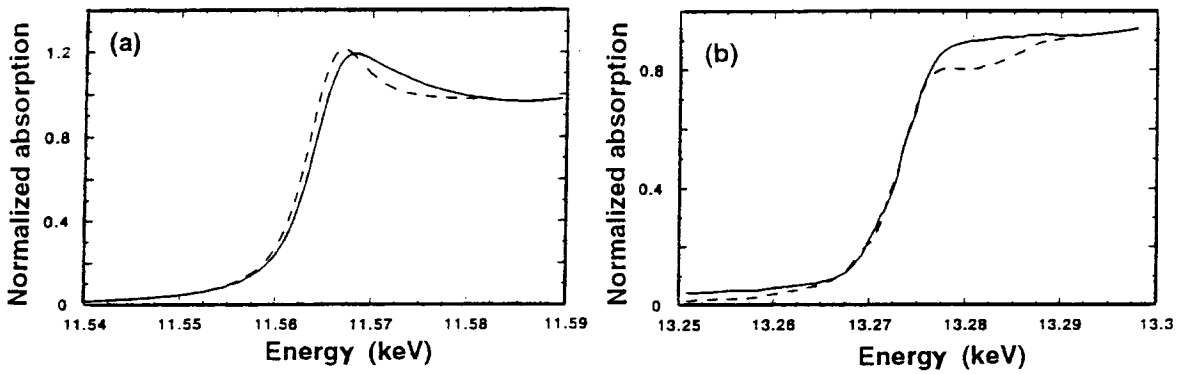

Figure X.20. — X-ray absorption edge of $Pt/\gamma\text{-}Al_2O_3$ after reduction at 450°C (solid line) and after subsequent evacuation at 450°C (dashed line). a) L_{III} and b) L_{II} edge.

Table X.6. — EXAFS Pt-Pt coordination numbers and whiteline intensities of $Pt/\gamma\text{-}Al_2O_3$.

Teatment	N	ΔA_3	ΔA_2	Δh_T
Reduction 300°C	5.0	0.57	1.58	5.23
Evacuation 300°C	3.8	-0.58	-0.15	-1.70
Hydrogen 200°C	4.9	0.48	1.43	4.66
Reduction 450°C	5.0	0.35	1.14	3.64
Evacuation 450°C	4.1	-0.09	0.26	0.44

X.4.3.3. Influence of chemisorbed hydrogen on the white line intensity

The influence of chemisorbed hydrogen on the position and intensity of the white line has been investigated for the $Pt/\gamma\text{-}Al_2O_3$ sample reduced at 300 and 450°C. The Pt L_{III} and L_{II} X-ray absorption edges of after reduction at 300°C, evacuation at 300°C, heating in hydrogen to 200°C are shown in Figure X.18. Removal of chemisorbed hydrogen causes a dramatic decrease in the intensity of both the Pt L_{III} and L_{II} X-ray absorption edge. The white line intensity is completely restored by readmission of hydrogen at RT and subsequent heating to 200°C. The L_{III} edge of the evacuated sample is shifted to lower energies by -1.5 eV. Readmission of hydrogen causes an upward shift of 1.4 eV, almost completely restoring the original edge position. The L_{II} edge of the evacuated sample does not show the downward shift. In addition to the position change of the L_{III} edge, also a change in shape (sharpening) is evident upon removal of the chemisorbed hydrogen. The difference between these spectra and the corresponding X-ray absorption edge of platinum foil are plotted in Figure X.19, results of the numerical integration of these curves between -2 and 17 eV are listed in Table X.6.

The Pt L_{III} and L_{II} X-ray absorption edges after reduction at 450°C and subsequent evacuation at 450°C are shown in Figure X.20. Evacuation causes a downward shift of the position of the Pt L_{III} edge of -0.7 eV, which is approximately half the shift obtained for the sample reduced at 300°C. Again no shift of the L_{II} edge was observed. The results of the integration are listed in Table X.6. The decrease in white line intensity by removal of chemisorbed hydrogen is not as large as after reduction and evacuation at 300°C. Furthermore, the white line intensity in the presence of chemisorbed hydrogen is lower after reduction at 450°C than after reduction at 300°C.

X.4.4. Discussion

The removal of chemisorbed hydrogen leads to a decrease in white line intensity (i.e. a decrease in the number of unfilled d-states). This is in agreement with literature data (Lytle (2) et al., 1985; Samant et al., 1991; McHugh et al., 1990) where the whiteline is reported to be affected by the presence of either hydrogen or helium during the measurement. The larger decrease in white line intensity in our measurement compared to literature data originates from the smaller particles in this study. In smaller particles a larger fraction of the atoms is exposed to adsorbed gases and thus a larger effect of adsorbed gases on the white line intensity is to be expected.

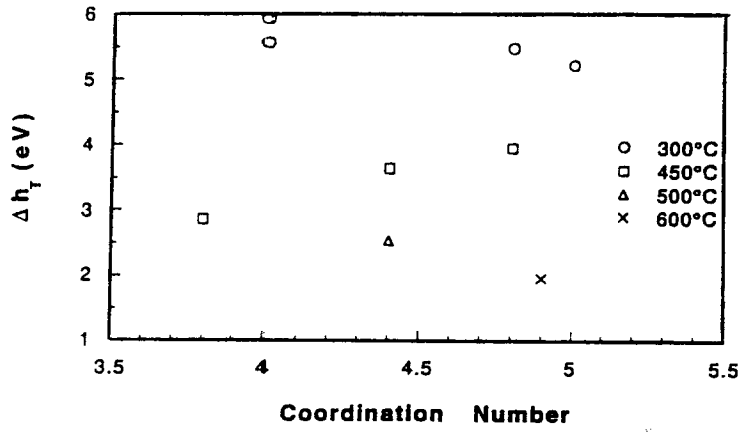

Figure X.21. — Correlation between first shell Pt-Pt coordination number and total number of unfilled d-states after reduction at 300 (squares), 450 (circels), 500 (triangle) and 600°C (cross) for different supported platinum catalysts.

After reduction and evacuation at 300°C the total number of unfilled d-states is less than the total number of unfilled d-states in the platinum foil (Δh_T = -1.7), indicating that the platinum particles have become electron rich in comparison to bulk platinum. In contrast, reduction and evacuation at 450°C results in a total number of unfilled d-states that is larger than the total number of unfilled d-states of platinum foil (Δh_T = 0.44), viz. the platinum particles are electron deficient in comparison to bulk platinum. The change in the number of unfilled d-states as a function of reduction temperature can not be explained by a change in particle size. The platinum particle size (= coordination number) did not change as a function of the reduction temperature. However, Vaarkamp (3) et al., 1993 showed that the structure of the metal-support interface changes when the reduction temperature is increased from 300 to 450°C. After reduction at 300°C hydrogen is present in the metal-support interface. In the absence of interfacial hydrogen, e.g. after reduction at 450°C, the interfacial platinum atoms are in direct contact with the support. The effect of the support on the number of unfilled d-states of supported platinum particles is not *a priori* known.

The results obtained by Vaarkamp (2), 1993 open for the first time the possibility to estimate the lower limit of the magnitude of the electron withdrawing or donating properties of γ-Al_2O_3 from or to small platinum particles. Intuitively, the removal of interfacial hydrogen is expected to have the same effect on the white line intensity as the removal of chemisorbed hydrogen, i.e. it is expected to decrease the white line intensity. Therefore it is logical to assume that removal of the interfacial hydrogen, (experimentally not possible after evacuation at 300°C !!) still present after evacuation at 300°C would lead to a further decrease of the white line intensity. After evacuation at 300°C Δh_T = -1.7. Removal of the interfacial hydrogen will then result in a further decrease of the white line intensity to a value lower than -1.7. An estimation can be made about a lower limit of this further decrease. The total decrease in the value of Δh_T due to the removal of chemisorbed hydrogen amounts about 7. For a platinum cluster of about 12 atoms at least 30% of the total amount of atoms will be present in the metal-support interface. Therefore, removal of interfacial

hydrogen would lead to a total value for Δh_T of at least -4. The white line intensity of the sample after evacuation at 450°C is found to be 0.44. This is caused by the influence of the support, since the interfacial platinum atoms are now in direct contact with the support. This counteracts the effect of the removal of interfacial hydrogen. The lower limit of the magnitude of the influence of the support can now be estimated to be at least 4.4, which is comparable with 7, the influence of chemisorbed hydrogen.

Vaarkamp (2), 1993 studied a number of different types of supported platinum catalysts. The changes of the number of unfilled d-states with the first shell Pt-Pt coordination number e.g. particle size, after reduction are shown in Figure X.21. It is evident that the changes in the number of unfilled d-states are mainly determined by the reduction temperature. The number of unfilled d-states for a particular reduction temperature is constant in the range of extremely small particles used in this study. A particle size effect is expected to be present when the range of particle sizes is extended to much larger particle (Yoshitaka et al., 1991). The decreases of the white line intensity with increasing reduction temperature can now be explained straightforward. Increasing the reduction temperature changes the structure of the metal-support interface and decreases the hydrogen chemisorption capacity (Vaarkamp (2) et al., 1993). The decrease in the amount of chemisorbed hydrogen decreases the white line intensity. This effect is apparently in the same order of magnitude as the effect of the change in the structure of the metal-support interface, e.g. increase in intensity due to the removal of interfacial hydrogen and an unknown effect of the support. Hence, to establish the effect of the support on the electronic structure of small metal particles, measurements in the absence of both chemisorbed and interfacial hydrogen should be performed. This has to be the subject of future research.

REFERENCES

ASHLEY C.A., DONIACH S., 1975 - Phys. Rev. B11, 1279.

BINSTED N., COOK S.L., EVANS J., GREAVES G.N., PRICE R.J., 1987 - J. Am. Chem. Soc. 109, 3669.

BOUDART M, DJEGA-MARIADASSOU, 1984 - Kinetics of Heterogenous Catalytic Reactions - Princeton University Press, Princeton N.J.

BROWN M., PEIERLES R.E., STERN E.A., 1977 - Phys. Rev. B15, 738.

BUNKER B.A., STERN E.A., 1983 - Phys. Rev. B27, 1017.

CITRIN P.H., EISENBERGER P., KINCAID B.M., 1976 - Phys. Rev. Lett. 22, 3551.

COOK Jr. J.W., SAYERS D.E., 1981 - J. Appl. Phys. 52, 5024.

van DIJK M.P., van VEEN J.A.R., BOUWENS S.M.A.M., van ZON F.B.M., KONINGSBERGER D.C., 1990 - Proc. 2nd European Conf. on Progress in X-Ray Synchrotron Radiation Research - SIF (Bologna) 139-142.

FONTAINE A., 1993 - Neutron and Synchrotron Radiation for Condensed Matter Studies, Vol I, Theory, Instruments and Methods - Springer-Verlag (Berlin) and Les Editions de Physique (Les Ulis, France).

GALLEZOT P., DATKA J., MASSARDIER J., PRIMET M., IMELIK B., 1977 - Proc. 6th Int. Congr. Catal., London 1976, - Chem. Society (London) 696.

GALLEZOT P., WEBER R., DALLA BETTA R.A., BOUDART M., 1979 - Z. Naturforsch A34, 40.

GORDON M.B., CYROT-LACKMANN F., DESJONQUERES M.C., 1977 - Surf. Sci. 68, 359.

HALLER G.L., RESASCO D.E., 1989 - Adv. Catal. 36, 173.

HENRICH V.C., 1985 - Rep. Progr. Phys. 48, 1481.

HORSLEY J.A., 1982 - J. Chem. Phys. 76, 1451.

McHUGH B.J., LARSEN G., HALLER G.L., 1990 - J. Phys. Chem. 94, 8621.

McKALE A.G., KNAPP G.S., CHAN S.-K., 1986 - Phys. Rev. B33, 841.

McKALE A.G., VEAL B.W., PAULIKAS A.P., CHAN S.-K., KNAPP G.S., 1988 - J. Am. Chem. Soc. 110, 3763.

KAMPERS F.W.H., 1989 - Exafs in Catalysis; Instrumentation and Applications - PhD Thesis, Eindhoven University of Technology.

KAMPERS F.W.H., MAAS T.M.J., van GRONDELLE J., BRINKGREVE P., KONINGSBERGER D.C., 1989 - Rev. Sci. Instr. 60, 2635.

KIP B.J., DUIVENVOORDEN F.B.M., KONINGSBERGER D.C., PRINS R., 1986 - J. Am. Chem. Soc. 108, 5633.

KIP B.J., DUIVENVOORDEN F.B.M., KONINGSBERGER D.C., PRINS R., 1987 - J. Catal. 105, 26.

KONINGSBERGER D.C., GATES B.C., 1992 - Catal. Lett. 14, 271.

LAMB H.H., GATES B.C., KNOEZINGER H., 1988 - Angew. Chem. Int. Ed. Engl. 27, 1127.

LEE P.A., PENDRY J.B., 1975 - Phys. Rev. B27, 95.

LENGELER B., 1986 - J. Phys. (Paris) 47, 75.

LYTLE F.W., 1976 - J. Catal. 43, 376.

LYTLE F.W., WEI P.S.P., GREGOR R.B., VIA G.H., SINFELT J.H., 1979 - J. Chem. Phys. 70, 4849.

LYTLE F.W.(1), GREEGOR R.B., MARQUES E.C., SANDSTROM D.R., VIA G.H., SINFELT J.H., 1985 - J. Catal. 95, 546.

LYTLE F.W.(2), GREEGOR R.B., MARQUES E.C., BIEBESHEIMER V.A., SANDSTROM D.R., HORSLEY J.A., VIA G.H., SINFELT J.H., 1985 - ACS Symp. Ser. 288, 280.

LYTLE F.W., SAYERS D.E., STERN E.A., 1988 - Physica B158, 701.

LYTLE F.W., GREEGOR R.B., 1990 - Appl. Phys. Lett. 56, 192.

MALONEY S.D., van ZON F.B.M., KELLEY M.J., KONINGSBERGER D.C., GATES B.C., 1990 - Catal. Lett. 5, 161.

MALONEY S.D., KELLEY M.J., KONINGSBERGER D.C., GATES B.C., 1991 - J. Phys. Chem. 95, 9406.

MANSOUR A.N., COOK Jr. J.W., SAYERS D.E., 1984 - J. Phys. Chem 88, 2330.

MARTENS J.H.A., PRINS R., ZANDBERGEN H., KONINGSBERGER D.C., 1988 - J. Phys. Chem. 92, 1903.

MATTHEISS L.F., DIETZ R.E., 1980 - Phys. Rev. B22, 1663.

MILLER J.T., MEYERS B.L., MODICA F.S., LANE F.S., VAARKAMP M., KONINGSBERGER D.C., 1993 - J. Catalysis, in press.

MOTT N.F., 1949 - Proc. Phys. Soc. London 62, 416.

MUSTRE DE LEON J., REHR J.J., ZABINSKY S.I., ALBERS R.C., 1991 - Phys. Rev. B44, 4146.

PENDRY J.B., 1974 - Low Energy Electron Diffraction - Academic Press (London).

RAVENEK W., JANSEN A.P.J., van SANTEN R.A., 1989 - J. Phys. Chem. 93, 6445.

SAILLARD J.Y., HOFFMANN R., 1984 - J. Am. Chem. Soc. 106, 2006.

SAMANT M.G., BOUDART M., 1991 - J. Phys. Chem. 95, 4070.

SAYERS D.E., 1987 - X-Ray Absorption: Principles, Applications, Techniques of Exafs, Sexafs and Xanes - John Wiley & Sons (New York), 211-253.

STERN E.A., SAYERS D.E., LYTLE F.W., 1975 - Phys. Rev. B11, 4836.

STEVENSON S.A., DUMESTIC J.A., RUCKENSTEIN E., Editors, 1987 - Metal-Support Interactions in Catalysis, Sintering and Redispersion - Van Nostrand Reinhold (New York).

TEO B.K., LEE P.A., 1979 - J. Am. Chem. Soc. 101, 2815.

VAARKAMP M.(1), DRING I., OLDMAN R.J., STERN E.A., KONINGSBERGER D.C., 1993 - Phys. Rev. B., in press.

VAARKAMP M. (2), 1993 - The Structure and Catalytic Properties of Supported Platinum Catalysts - PhD Thesis, Eindhoven University of Technology.

VAARKAMP M.(3), MODICA F.S., MILLER J.T., KONINGSBERGER, 1993- J. Catal., in press.

YOSHITAKE H., IWASAWA Y., 1991 - J. Phys. Chem. 95, 7368.

van ZON J.B.A.D., KONINGSBERGER D.C., van 't BLIK H.F.J., SAYERS D.E., 1985 - J. Chem. Phys. 82, 5742.

van ZON F.B.M., MALONEY S.D., GATES B.C., KONINGSBERGER D.C., 1993 - J. Amer. Chem. Soc., in press.